

Quantum Computation of Electronic Structure with Projector Augmented-Wave Method and Plane Wave Basis Set

Aleksei V. Ivanov,^{1,*} Andrew Patterson,¹ Marius Bothe,^{1,2} Christoph Sünderhauf,¹ Bjorn K. Berntson,¹ Jens Jørgen Mortensen,³ Mikael Kuisma,³ Earl Campbell,^{1,4} and Róbert Izsák¹

¹*Riverlane Ltd, St Andrews House, 59 St Andrews Street, Cambridge, CB2 3BZ, United Kingdom*

²*Astex Pharmaceuticals, 436 Cambridge Science Park, Cambridge, CB4 0QA, United Kingdom*

³*CAMd, Department of Physics, Technical University of Denmark, 2800 Kgs. Lyngby, Denmark*

⁴*Department of Physics and Astronomy, University of Sheffield, UK*

Quantum simulation of materials is a promising application area of quantum computers. In order to realize this promise, finding ways to reduce quantum resources while maintaining the accuracy of results will be necessary. In electronic structure calculations on classical computer the reduction of resources has been achieved by using the projector augmented-wave method (PAW) and plane wave basis sets. In this work, we present an implementation of the PAW with plane waves for quantum computation of the energy. We first generalize the approach to many-body wavefunctions and develop the unitary version of the PAW which preserves the orthonormality of orbitals. Then, we provide a linear-combination-of-unitaries decomposition which explicitly accounts for the atomic two-body PAW correction and provide the corresponding block encodings of the Hamiltonian used in qubitized quantum phase estimation. We then estimate quantum resources for crystalline solids using down-sampling to estimate the energy within chemical accuracy with respect to the full basis set limit, and also consider a supercell approach which is more suitable for calculations of defect states. We provide the quantum resources for energy estimation of a nitrogen-vacancy defect centre in diamond which is a challenging system for classical algorithms and a quintessential problem in the studies of quantum point defects.

CONTENTS

I. Introduction	2
II. Many-body Projector Augmented-Wave Method	4
A. Unitary Projector Augmented-Wave method	6
III. Hamiltonian in second quantization	8
IV. Block encoding	10
V. Results	11
A. Space and Time Complexity of the Quantum Algorithm	11
B. Quantum Resource Estimates	13
1. Crystalline solids	13
2. Defects in Solids. Nitrogen-Vacancy Centre in Diamond.	15
VI. Discussion and Conclusion	17
VII. Acknowledgement	18
A. Compression of virtual space with approximate MP2-natural orbitals	19
B. Matrix elements in PAW formalism and plane wave basis set	19
1. Factorization of soft two-body term using plane waves	20
2. Factorization of PAW two-body part	21
C. Quantum Error Correction	22

* Corresponding author: aleksei.ivanov@riverlane.com

D. Properties of reciprocal pair densities	22
1. Complex orbital-pair densities	22
2. Real orbital-pair densities	23
E. Block encoding of a squared matrix	23
References	23

I. INTRODUCTION

Ab initio simulation of electronic structure is of great importance since it enables the discovery of new materials and the interpretation of experimental data that would be otherwise impossible. For such simulations to be truly predictive, they need to have controllable errors in their approximations to deliver high-accuracy results. While there has been tremendous progress in developing classical heuristics, they still have limitations that quantum computation promises to overcome.

Conceptually, there are two important sources of error in electronic structure calculations, not considering relativity and other more specific effects. The first error source originates in approximating the N -electron wavefunction, and the simplest approximation is a (antisymmetrized) product of N one-electron wavefunctions (orbitals). Variational optimization of such an ansatz leads to the Hartree-Fock (HF) integro-differential equations. The difference between energies calculated at the HF level and at the exact level is called the correlation energy and the associated correlation problem is at the heart of traditional quantum chemistry [1]. If HF is a good initial guess, then various classical heuristics usually provide an accurate enough description of the physical system involved [1, 2]. Classical approaches struggle much more with systems where correlation effects are strong, and the HF ansatz has small overlap with the true ground state wavefunction. The popular Kohn-Sham density functional theory (KS-DFT) [3] also relies on the single Slater determinant approximation and while it is capable of capturing some correlation effects, KS-DFT also struggles with strong correlations when the density cannot be approximated by the density of a single Slater determinant. As such, strongly correlated electrons are natural systems to seek advantage in quantum computation.

The second source of error comes from the finite basis expansion or discretization of the computational problem. The HF equations, in the form discussed so far, can only be solved for the simplest of problems. Thus, the orbitals themselves are usually expanded as a linear combination of known basis functions. This leads to the algebraic Hartree-Fock or Hartree-Fock-Roothaan equations [4] which can be solved for much larger systems. A good basis set has the property that the energy rapidly converges to the exact solution, the so-called basis set limit, as the number of basis functions grows. The rate of this convergence depends on the basis set used, so a prudent choice is of paramount importance for computational efficiency. Historically, the inspiration for such a choice usually came from analytic solutions available for simple systems. For molecules, the analytical solutions of the Schrödinger equation for the H atom first inspired Slater type orbitals (exponentials) and later Gaussian type orbitals [5] centered on every atom in the molecule and hence called atomic orbitals (AO). The choice of Gaussians is motivated by the fact that the resulting integrals can be evaluated efficiently in contrast with Slater type orbitals, which converge faster to the basis set limit. In both cases, fast decay of the wavefunction at large distances reflects the physical nature of the problem: molecules represent finite multi-center versions of the single centre potential in the H atom. However, for metals the reference system is the free electron gas, which has an analytic solution, namely plane waves (PW) [6]. The free electron gas is a good initial approximation of valence electrons in metals and PW also reflect an important characteristic of solids: they are (infinitely) extended. Thus, it is not surprising that plane waves are the *de facto* choice of basis for the accurate simulation of periodic systems [7] even though it is possible to use localized AO basis sets in solid state calculations and, vice versa, PW in molecular ones, sometimes with benefit due to some favourable property. Advantages of PW include: they provide an unbiased description of ground and excited states (which eases calculation of optical properties); and they are free of basis set superposition error (a principle error source in atomic orbitals like Gaussians). Thus, using plane waves for quantum computation would be beneficial for high precision calculations.

Quantum algorithms employing plane wave and dual plane-wave basis sets for all-electron (i.e. when both core and valence electrons are treated at equal footing) second-quantized electronic structure calculations have been developed in Refs [8–10]. However, such all-electron simulations would require an extremely large number of plane wave coefficients (high kinetic energy cutoffs) and therefore a large number of qubits and gates to carry out practical simulations on quantum computers. For example, Gygi carried out all-electron plane wave KS-DFT calculations with a *regularized* Coulomb potential [11] and have shown that in the case of Silicon the convergence of the eigenvalues with accuracy up to 0.01 eV requires a kinetic energy cutoff to be around 60-80 kRy (80 kRy $\approx 10^6$ eV), which for a small cubic unit cell with volume of 1 Å³ corresponds to around 2×10^6 plane wave coefficients. For a true Coulomb

potential this number would be even larger and will increase for larger elements. In classical computation, a reduction in the number of plane-wave coefficients has been achieved by using either pseudopotentials [12, 13] or the projector augmented-wave (PAW) method [14]. In the PAW approach, one constructs the PAW operator, $\hat{\mathcal{T}}$, which allows one to carry out a transformation between all-electron wavefunctions, which exhibit strong oscillations and cusps around nuclei, and pseudo orbitals, which are smooth functions close to nuclear regions. Results of such PAW transformations are shown in Fig. 1. The efficiency and precision of the PAW transformation then depends on the practical procedure used to construct such operators. The PAW method is the most accurate approach used in condensed matter simulations and often requires considerably fewer plane waves. In density functional theory, such reduction in the number of plane waves can be expected to be up to 3–4 orders of magnitude w.r.t all-electron simulations and a factor of 2–3 w.r.t. norm-conserving pseudopotentials [15]. Benchmarks on density functional approximations and many-body theories for molecules indicate that the error due to PAW calculations can be well below chemical accuracy [16, 17]. The electronic structure software based on the PAW approach also show better precision and efficiency than pseudopotentials, such as norm-conserving pseudopotentials [15, 18, 19]. While the Goedecker-Teter-Hutter norm-conserving pseudopotentials [20, 21] have recently been implemented for quantum computation with plane wave basis sets in first quantization [22–24], in this work, we will show an implementation of the PAW method with the frozen-core approximation, and adapt the Hamiltonian in a convenient form for quantum computation in second quantization. Since quantum computing is expected to be used for high-precision calculations, the errors introduced by approximations to the Hamiltonian and the wavefunction must be within the allowable error budgets and thus, given the efficiency and precision of PAW, this approach is more favorable than other pseudopotentials for quantum computation, requiring smaller basis sets.

The PAW method is an all-electron approach which is exact in theory [14] but relies on several approximations in practice. Together with its advantages it brings additional complications in the implementation, one of which is that the electronic integrals are not generally analytically computable in the PAW formalism and one usually has to work with non-orthogonal orbitals. To overcome complications introduced by non-orthogonal orbitals, we develop a unitary version of PAW setups (the UPAW approach) and formulate a many-body PAW transformation for the generic chemistry Hamiltonian in first and second quantization in Sec. II.

The quantum algorithm we consider in this work is qubitization-based [25–27] quantum phase estimation (QPE) [28, 29]. The starting point is the decomposition of the Hamiltonian into a linear combination of unitaries (LCU):

$$(I.1) \quad \hat{H} = \sum_{l=0}^{L-1} \omega_l \hat{W}_l,$$

where ω_l are real numbers, and \hat{W}_l are unitary matrices. The operator used in qubitized QPE is the block-encoding of the Hamiltonian; an embedding of \hat{H} into a larger unitary matrix \hat{V} :

$$(I.2) \quad \hat{V} = \begin{pmatrix} \hat{H}/\lambda & \text{junk}_1 \\ \text{junk}_2 & \text{junk}_3 \end{pmatrix}.$$

The subnormalization factor λ is often closely related to the one-norm $\lambda = \sum_{l=0}^{L-1} |\omega_l|$ of the Hamiltonian’s LCU on which the block encoding is based. The asymptotic complexity of qubitized QPE is then determined by Γ , the amount of information needed to specify the LCU decomposition (I.1), and λ . Using a QROAM (also known as select-swap network) [30, 31] for data loading, the Toffoli complexity is $O(\sqrt{\Gamma}\lambda/\epsilon_{\text{QPE}})$ and the qubit number complexity is $O(\sqrt{\Gamma})$, where ϵ_{QPE} is the error budget in the QPE [31]. As one can see, the properties of the LCU determine the efficiency of the quantum algorithm, and thus developing an LCU decomposition which lowers the overall cost is of great importance. Several such decompositions and corresponding block encodings of the Hamiltonian have been proposed in the past for molecular systems [31–33] and more recently generalized for periodic solids [34, 35] based on Gaussian basis sets. In this work, we will use the plane wave decomposition and unitary PAW approach to construct an explicit LCU in second quantization and the corresponding block encoding. We note in passing that our implementation is also valid for norm-conserving pseudopotentials since the latter can be implemented as the PAW method with several parameters set to zeros [36].

In order to estimate the energy of periodic solids at the converged basis set limit, one can use a popular strategy developed in classical computation called the down-sampling technique [37, 38]. There, the energy of the system can be estimated using energy differences with a smaller number of orbitals which results in lower computation resources to estimate energy at the converged basis set limit. Naturally, the question arises if such a technique would provide feasible quantum resources for ground-state energy estimation. We will explore this question in Sec. V.

To summarise, the results of this work are: (i) We introduce the unitary PAW method, a generalization of PAW for many-body wavefunctions which allows for calculations with chemical accuracy; (ii) We present LCU decomposition of the Hamiltonian in second quantization using PAW and plane waves and use it in qubitization-based QPE. Our

asymptotic scalings are similar to those from double-factorization based on a Cholesky decomposition [32] when the system grows towards the thermodynamic limit; (iii) We carry out resource estimation for diamond using the down-sampling technique for calculating the energy within chemical accuracy with respect to the full basis set limit; (iv) Finally, we also consider the nitrogen-vacancy centre in diamond – a challenging system for classical algorithms, and provide the resource estimates for this system too.

The paper is organized as follows. In Sec. II, we introduce the many-body PAW transformation as well as a unitary version of the method. In Sec. III, we present an LCU decomposition using the plane-wave basis set and the projector augmented-wave method. In Sec. IV, we outline the modification of quantum circuits from the double-factorization method to our setting. In Sec. V, we numerically determine asymptotic scalings of the quantum computational time and space cost of our algorithm. Further, we show quantum resource estimates for periodic solids. In Sec. VI, discussion and conclusion are presented.

II. MANY-BODY PROJECTOR AUGMENTED-WAVE METHOD

Within the Born-Oppenheimer approximation, the motion of electrons and nuclei are decoupled and the electrons are described using the clamped-nuclei approach, i.e., the electrons move in the field generated by nuclei with charges $\{Z_a\}$ fixed at the positions $\{\mathbf{P}_a\}$. The resulting Hamiltonian can be written as

$$(II.1) \quad \hat{H} = \sum_{a>b}^{N_A} \frac{Z_a Z_b}{|\mathbf{P}_a - \mathbf{P}_b|} + \sum_{j=1}^N \left(-\frac{1}{2} \nabla_j^2 - \sum_{a=1}^{N_A} \frac{Z_a}{|\mathbf{r}_j - \mathbf{P}_a|} \right) + \sum_{j>m}^N \frac{1}{|\mathbf{r}_j - \mathbf{r}_m|}$$

$$(II.2) \quad = C + \sum_{j=1}^N \hat{h}_j + \sum_{j>m}^N \hat{g}_{jm},$$

where N is the number of electrons, N_A is the number of atomic centers (nuclei). Apart from the Laplacian ∇_j^2 , which is a differential operator appearing in the kinetic energy term for electron j , the potential terms are multiplication operators \hat{V} that multiply the functions $f(\{\mathbf{r}_j\})$ they act on by a potential function of the form $V(\{\mathbf{r}_j\})$, i.e., $\hat{V}f(\{\mathbf{r}_j\}) = V(\{\mathbf{r}_j\})f(\{\mathbf{r}_j\})$, where $\{\mathbf{r}_j\}$ are the spatial coordinates of the electrons. The constant term C consists of the nuclear repulsion term, the one-electron operator \hat{h}_j acts on the j th electron and contains the kinetic energy contribution of that electron and its potential energy at position \mathbf{r}_j in the field of all the nuclei, and finally, the two-electron terms \hat{g}_{jm} merely consists of the repulsion between electrons. The goal is to estimate the ground state energy E of the Hamiltonian:

$$(II.3) \quad \hat{H}\Psi(\mathbf{x}_1, \dots, \mathbf{x}_N) = E\Psi(\mathbf{x}_1, \dots, \mathbf{x}_N),$$

where $\mathbf{x} = (\mathbf{r}, \sigma)$ is a combined coordinate variable consisting of the spatial (\mathbf{r}) and spin (σ) degrees of freedom. In order to solve this equation, the wavefunction Ψ is expressed in terms of orbitals, such as plane waves. Because the wavefunction demonstrates rapid oscillations near the nuclei, one would need a large number of plane waves. In order to reduce the number of plane wave coefficients, we generalize the projector augmented-wave (PAW) method [14] [see Ref. [39] for a summary], which was originally developed for density functional theory calculations, for many-body wavefunctions.

The key feature of the PAW approach is that it establishes a linear transformation $\hat{\mathcal{T}}$ between a set of Hartree-Fock or Kohn-Sham orbitals $\{\psi(\mathbf{x})\}$ and a set of smooth pseudo orbitals $\{\tilde{\psi}(\mathbf{x})\}$ that have no cusps around the nuclei,

$$(II.4) \quad \psi(\mathbf{x}) = \hat{\mathcal{T}}\tilde{\psi}(\mathbf{x}).$$

Crucially, the orbitals and the transformation operator itself are then constructed from atomic contributions. To achieve this, the system is divided into atom-centered augmentation spheres within which $\psi(\mathbf{x})$ is expanded in terms of localized (atom-like) partial waves $\phi_j^a(\mathbf{r})$, where j identifies one such function belonging to the atom labelled by a . Similarly, the pseudo orbitals $\tilde{\psi}(\mathbf{x})$ are also expanded using smooth pseudo partial waves denoted as $\tilde{\phi}_j^a(\mathbf{r})$. The functions $\phi_j^a(\mathbf{r})$ and $\tilde{\phi}_j^a(\mathbf{r})$ are identical outside the augmentation sphere around atom a , and they are related by the transformation $\hat{\mathcal{T}}$ in the same way as the orbitals $\psi(\mathbf{x})$ and $\tilde{\psi}(\mathbf{x})$. As a result, the atomic-centre expansion of orbitals can be given as [14]:

$$(II.5) \quad \psi(\mathbf{x}) = \tilde{\psi}(\mathbf{x}) + \sum_{a=1}^{N_A} \sum_{j=1}^{n_a} (\phi_j^a(\mathbf{r}) - \tilde{\phi}_j^a(\mathbf{r})) \int_V d^3\mathbf{r}' \tilde{p}_j^a(\mathbf{r}') \tilde{\psi}(\mathbf{x}').$$

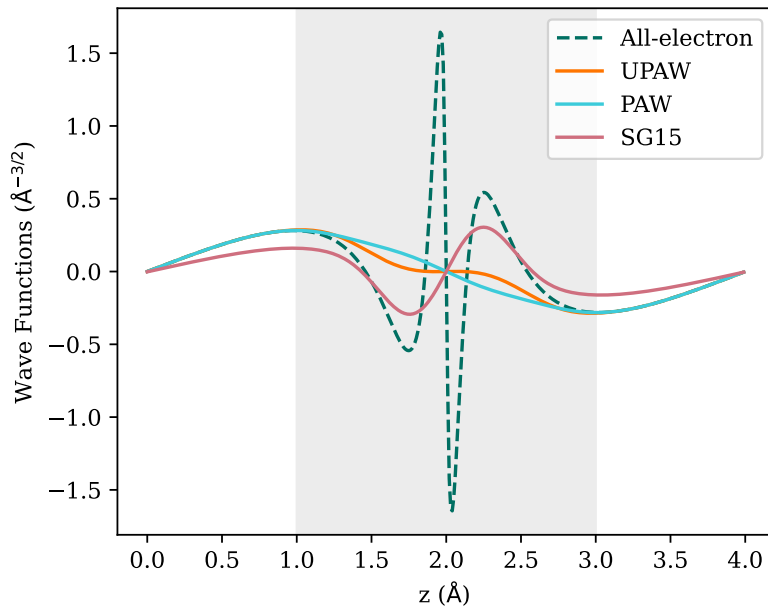


FIG. 1. **All-electron and pseudo orbitals obtained using PAW [14], UPAW [this work] and norm-conserving Vanderbilt pseudopotential (SG15) [40].** Orbitals (lowest unoccupied orbitals + 1) obtained from calculations of Ni atom using 800 eV kinetic energy cutoff. The grey interval indicates an area outside of which the all-electron and (U)PAW orbitals are the same. In 3D, this interval would instead be a ball.

Here, n_a is the total number of projector functions, $\{\tilde{p}_j^a(\mathbf{r}')\}$, localized on an atom a , which can be constructed from any set of linearly independent functions and which must be biorthogonal to pseudo partial waves [14]. The integration domain in Eq. B.25, V , is a cell in the case of a periodic solid, or is \mathbb{R}^3 for an isolated molecule. To simplify our notation, the combined index $k = (a, j)$ will be introduced as well as the functions:

$$(II.6) \quad \chi_k(\mathbf{r}) = \phi_k(\mathbf{r}) - \tilde{\phi}_k(\mathbf{r}).$$

Both $\chi_k(\mathbf{r})$ and $\tilde{p}_k(\mathbf{r})$ are localized at the nuclei, a , and vanish outside the augmentation ball, \mathbb{B}_a . The PAW operator, $\hat{\mathcal{T}}$ acting on the pseudo orbitals is then defined as

$$(II.7) \quad \hat{\mathcal{T}} = \hat{I} + \sum_k \hat{\mathcal{T}}_k,$$

where $\hat{\mathcal{T}}_k$ is an integral operator defined by its action on the test function $f(\mathbf{r})$ as

$$(II.8) \quad \hat{\mathcal{T}}_k f(\mathbf{r}) = \chi_k(\mathbf{r}) \int_V d^3\mathbf{r}' \tilde{p}_k(\mathbf{r}') f(\mathbf{r}').$$

Since the spin orbitals $\psi(\mathbf{x})$ are products of a spatial part of the form $f(\mathbf{r})$ and a pure spin part depending on the spin variable σ , it should be noted that when $\hat{\mathcal{T}}_k$ acts on $\psi(\mathbf{x})$ it leaves the spin part entirely unaffected. This can be expressed in the bra-ket notation as:

$$(II.9) \quad \hat{\mathcal{T}} = \hat{I} + \sum_k |\chi_k\rangle \langle \tilde{p}_k| \otimes I_s,$$

where I_s is identity operator acting on spin degrees of freedom. As an example, we show the results of the PAW transformation in Fig. 1.

Next, we show how to generalize the PAW transformation to a many-body wavefunction, Ψ . In order to do this, we follow a procedure, similar to the configuration interaction expansion [41, p.251], in which the PAW transformation is applied recursively coordinate by coordinate:

$$(II.10) \quad \Psi_{j-1}(\mathbf{x}_1, \mathbf{x}_2, \dots, \mathbf{x}_N) = \Psi_j(\mathbf{x}_1, \mathbf{x}_2, \dots, \mathbf{x}_N) + \sum_{k_j} \chi_{k_j}(\mathbf{r}_j) \int d\mathbf{r}'_j \tilde{p}_{k_j}(\mathbf{r}'_j) \Psi_j(\mathbf{x}_1, \dots, \mathbf{x}'_j, \dots, \mathbf{x}_N), \quad j = 1 \dots N,$$

Ψ_0 is the original many-body wavefunction and Ψ_N is a smooth many-body wavefunction which does not have cusps around the nuclei,

$$(II.11) \quad \Psi_0(\mathbf{x}_1, \mathbf{x}_2, \dots, \mathbf{x}_N) := \Psi(\mathbf{x}_1, \mathbf{x}_2, \dots, \mathbf{x}_N),$$

$$(II.12) \quad \Psi_N(\mathbf{x}_1, \mathbf{x}_2, \dots, \mathbf{x}_N) := \tilde{\Psi}(\mathbf{x}_1, \mathbf{x}_2, \dots, \mathbf{x}_N).$$

Using this recursive relation, one obtains the many-body PAW transformation:

$$(II.13) \quad \hat{\mathcal{T}}_{MB} = \hat{\mathcal{T}}(1) \otimes \hat{\mathcal{T}}(2) \otimes \dots \otimes \hat{\mathcal{T}}(N) = I + \sum_{i_1} \sum_{k_1} |\chi_{k_1}(i_1)\rangle \langle \tilde{p}_{k_1}(i_1)| + \\ + \sum_{i_1 < i_2} \sum_{k_1 < k_2} |\chi_{k_1}(i_1)\chi_{k_2}(i_2)\rangle \langle \tilde{p}_{k_1}(i_1)\tilde{p}_{k_2}(i_2)| + \dots + \sum_{k_1 < \dots < k_N} |\chi_{k_1}(1)\dots\chi_{k_N}(N)\rangle \langle \tilde{p}_{k_1}(1)\dots\tilde{p}_{k_N}(N)|,$$

where $|\chi_{k_1}(1)\dots\chi_{k_N}(N)\rangle$, $|\tilde{p}_{k_1}(1)\dots\tilde{p}_{k_N}(N)\rangle$ are the Slater determinants, and the PAW-transformed Schrödinger equation for the pseudo many-body wavefunction can be written as follows:

$$(II.14) \quad \hat{H}|\tilde{\Psi}\rangle = E\hat{S}|\tilde{\Psi}\rangle,$$

with

$$(II.15) \quad \hat{H} = \hat{\mathcal{T}}_{MB}^\dagger \hat{H} \hat{\mathcal{T}}_{MB},$$

$$(II.16) \quad \hat{S} = \hat{\mathcal{T}}_{MB}^\dagger \hat{\mathcal{T}}_{MB}.$$

and E is the same energy as in the all-electron Schrödinger Equation (II.3). While the wavefunction becomes smooth around nuclei, the PAW transformation brings additional complications. First, the eigenstates of the Hamiltonian are not orthonormal anymore, that is:

$$(II.17) \quad \langle \tilde{\Psi}_i | \tilde{\Psi}_j \rangle \neq \delta_{ij}.$$

As a result, one has to solve a generalized eigenvalue problem. Secondly, the PAW transformation generally leads to an N -body interaction term unless one implements the inverse PAW transformation, $\hat{\mathcal{T}}_{MB}^{-1}$. This complicates the use of orthonormal basis sets such as plane waves, while the use of non-orthogonal basis functions complicates the mathematical description of many-body techniques. In order to overcome these shortcomings we develop the *unitary* PAW method (UPAW) which eliminates the complications of a conventional PAW method.

A. Unitary Projector Augmented-Wave method

In our unitary variant, the general structure of the PAW method will be largely unchanged. Modifications are introduced at the level of constructing pseudo partial waves. We would like to make $\hat{\mathcal{T}}$ a unitary operator, $\hat{\mathcal{T}}^\dagger = \hat{\mathcal{T}}^{-1}$. This means that the one-electron overlap operator:

$$(II.18) \quad \hat{O} = \hat{\mathcal{T}}^\dagger \hat{\mathcal{T}} = I + \Delta\hat{O},$$

where

$$(II.19) \quad \Delta\hat{O} = \sum_a \sum_{i,j} |\tilde{p}_i^a\rangle O_{ij}^a \langle \tilde{p}_j^a|,$$

$$(II.20) \quad O_{ij}^a = \langle \phi_i^a | \phi_j^a \rangle - \langle \tilde{\phi}_i^a | \tilde{\phi}_j^a \rangle,$$

becomes the identity. This requires us to choose pseudo partial waves $\tilde{\phi}_i^a$ in such a way that O_{ij}^a is zero:

$$(II.21) \quad \langle \tilde{\phi}_i^a | \tilde{\phi}_j^a \rangle = \langle \phi_i^a | \phi_j^a \rangle.$$

We note that one possible way to enforce the orthogonality conditions (II.21) is to make both the partial and pseudo partial waves orthogonal, but such an approach would create additional oscillations of the wavefunction which would in turn increase the required number of plane-wave coefficients. In order to construct the pseudo partial waves without making them orthogonal we have developed the following procedure. The partial and pseudo partial waves are atomic-like orbitals, $\phi_i(\mathbf{r}) = r^l R_{nlp}(r) Y_{lm}(\hat{\mathbf{r}})$, where n is the principle quantum number, l is the angular momentum, m is magnetic quantum number and p is an additional index enumerating the number of partial waves per angular momentum value. While partial waves are solutions of the atomic Schrodinger equation, the pseudo partial waves $\tilde{\phi}_i^a$ are constructed to satisfy the properties:

1. The radial part of $\tilde{\phi}_i^a(\mathbf{r})$, $\tilde{R}_{nlp}(r)$, is a smooth function for $r \in \mathbb{B}_a$.
2. $\tilde{R}_{nlp}(r) = R_{nlp}(r)$ for $r \in \overline{\mathbb{B}}_a$.
3. At the boundary, we require $\partial^i \tilde{R}_{nlp}(r_a) = \partial^i R_{nlp}(r_a)$, $i \in \{0, 1, \dots, P-1\}$.
4. $O_{ij}^a = 0$ for any i, j, a .

We use the polynomial approximation to the radial part of pseudo partial waves inside the augmentation spheres:

$$(II.22) \quad R(r) = \sum_{p=0}^{P+M-1} (r^2)^{P+M-1-p} c_p,$$

where we allocate M coefficients to satisfy the orthonormality constraints (4). In order to find coefficients, c_p , non-linear optimization is carried out until the constraints (1-4) are satisfied. In order to improve the smoothness of pseudo partial waves, for some elements the optimization procedure also attempts to remove high Fourier components related to pseudo partial waves. Namely, let $b_i^a(\mathbf{G})$ be the Fourier transform of $r\tilde{\phi}_i^a(\mathbf{r})$, then we set $\sum_{|\mathbf{G}| > G_{max}} |\mathbf{G}|^2 |b_i^a(\mathbf{G})|^2 = 0$, where G_{max} is a parameter. The quality of the produced UPAW setups for some chemical elements will be shown in Sec. V. With the construction of the pseudo partial waves now described, we next continue with the formulation of the many-body problem.

For the unitary PAW transform, the pseudo many-body Schrödinger equation becomes

$$(II.23) \quad \hat{H}\tilde{\Psi} = E\tilde{\Psi},$$

where

$$(II.24) \quad \hat{H} = C + \sum_{j=1}^N \hat{\mathcal{T}}(j)^\dagger \hat{h}_j \hat{\mathcal{T}}(j) + \frac{1}{2} \sum_{i \neq j}^N \hat{\mathcal{T}}^\dagger(i) \hat{\mathcal{T}}^\dagger(j) \hat{g}_{ij} \hat{\mathcal{T}}(i) \hat{\mathcal{T}}(j) = C + \sum_{j=1}^N \hat{h}_j + \frac{1}{2} \sum_{i \neq j}^N \hat{g}_{ij}.$$

For practical applications, one has to evaluate the matrix elements of the Hamiltonian in either first or second quantization:

$$(II.25) \quad \hat{H} = C + \sum_i^N \sum_{p,q}^\infty h_{pq} \sum_\sigma (|\tilde{p}\sigma\rangle \langle \tilde{q}\sigma|)_i + \frac{1}{2} \sum_{i \neq j}^N \sum_{p,q,r,s}^\infty \kappa_{qprs} \sum_{\sigma,\tau} (|\tilde{p}\sigma\rangle \langle \tilde{q}\sigma|)_i (|\tilde{r}\tau\rangle \langle \tilde{s}\tau|)_j,$$

and

$$(II.26) \quad \hat{H} = C + \sum_{p,q,\sigma} h_{pq} \hat{a}_{p\sigma}^\dagger \hat{a}_{q\sigma} + \frac{1}{2} \sum_{pqrs;\sigma,\tau} \kappa_{qprs} \hat{a}_{p\sigma}^\dagger \hat{a}_{r\tau}^\dagger \hat{a}_{s\tau} \hat{a}_{q\sigma},$$

respectively. In the expression above, we used a spin-restricted approach and an orthonormal smooth basis set $\{|\tilde{p}\sigma\rangle\}$, where each function is labelled by a number \tilde{p} and spin index σ . The one- and two-body matrix elements calculated from the PAW-transformed one- and two-body operators are:

$$(II.27) \quad h_{pq} = \langle \tilde{p} | \hat{\mathcal{T}}^\dagger \hat{h} \hat{\mathcal{T}} | \tilde{q} \rangle,$$

$$(II.28) \quad \kappa_{qprs} = \langle \tilde{p} | \langle \tilde{r} | \hat{\mathcal{T}}^\dagger \otimes \hat{\mathcal{T}}^\dagger \hat{g} \hat{\mathcal{T}} \otimes \hat{\mathcal{T}} | \tilde{q} \rangle | \tilde{s} \rangle,$$

where \hat{h} and \hat{g} are conventional one- and two-body operators which in the $|\mathbf{r}\rangle$ basis can be written as:

$$(II.29) \quad \langle \mathbf{r}' | \hat{h} | \mathbf{r} \rangle = -\frac{1}{2} \nabla_{\mathbf{r}}^2 \delta(\mathbf{r} - \mathbf{r}') - \sum_{a=1}^{N_A} \frac{Z_a}{|\mathbf{r} - \mathbf{P}_a|} \delta(\mathbf{r} - \mathbf{r}')$$

$$(II.30) \quad \langle \mathbf{r}_1 \mathbf{r}_2 | \hat{g} | \mathbf{r}_3 \mathbf{r}_4 \rangle = \delta(\mathbf{r}_1 - \mathbf{r}_3) \delta(\mathbf{r}_2 - \mathbf{r}_4) \frac{1}{|\mathbf{r}_1 - \mathbf{r}_2|}$$

The operators, $|\tilde{p}\sigma\rangle \langle \tilde{q}\sigma|$, $\hat{a}_{p\sigma}^\dagger \hat{a}_{q\sigma}$ in Eqs. (II.25),(II.26), act directly on the pseudo many-body wavefunctions that require a significantly smaller number of basis functions, especially if plane wave basis sets are used. In this work, we focus on the Hamiltonian in second quantization, while first quantization will be considered in future work.

III. HAMILTONIAN IN SECOND QUANTIZATION

In the following, we will use the frozen-core approximation [42], where only valence and sometimes semicore electrons are explicitly considered. While the energetic contributions from the core electrons change the constant and the one-body terms, they are absent in the two-body term. It is also convenient to rewrite the Hamiltonian in terms of the generators of the unitary group $U(n)$ [43], i.e., spin-summed excitation operators (excitons)

$$(III.1) \quad \hat{E}_{pq} = \sum_{\sigma=0,1} \hat{a}_{p\sigma}^\dagger \hat{a}_{q\sigma}.$$

This yields a spin-free formulation in which all dependence on the spin is included in the summation in \hat{E}_{pq} :

$$(III.2) \quad \hat{H} = H^{(0)} + \sum_{pq} \left(h_{pq} - \frac{1}{2} \sum_r \kappa_{rprq} \right) \hat{E}_{pq} + \frac{1}{2} \sum_{pqrs} \kappa_{pqrs} \hat{E}_{pq}^\dagger \hat{E}_{rs},$$

where summations run over band indices p, q, r, s and the total number of bands is N_b . h_{pq} , κ_{rprq} are the matrix elements which are calculated using some orbitals, $\{\tilde{\psi}_p\}_{p=1}^{N_b}$. Crucially, the ground-state energy will depend on the number of orbitals, N_b , and this number should be large enough to ensure sufficient convergence up to an acceptable error (relative to the $N_b \rightarrow \infty$ energy). In computational quantum chemistry, the standard choice of orbitals is either canonical Hartree-Fock or Kohn-Sham orbitals, which are obtained by solving the one-electron Schrodinger equation

$$(III.3) \quad \hat{h} \tilde{\psi}_p(\mathbf{r}) = \epsilon_p \tilde{\psi}_p(\mathbf{r}), \quad p = 1 \dots N_b.$$

It is hard to solve these equations exactly without any numerical approximation, and this is why, additional basis functions, $\chi_g(\mathbf{r})$, are introduced to expand orbitals:

$$(III.4) \quad \tilde{\psi}_p(\mathbf{r}) = \sum_g^{N_g} \chi_g(\mathbf{r}) C_{gp}.$$

One then can rewrite Eq. III.3 in an algebraic form that is easier to solve on a classical computer.

As one can see, there are now two parameters N_g and N_b . N_g should be large enough so as to give a good approximation to $\tilde{\psi}_p(\mathbf{r})$ and N_b should be large enough so as to estimate the ground state energy of the Hamiltonian III.2 to a good accuracy. Usually, in practice $N_b = N_g$ especially when one employs Gaussian basis functions. But the condition $N_b = N_g$ might be too strict, for example if one uses natural orbitals instead of canonical orbitals with a plane wave basis set, in which case $N_b \ll N_g$ [38]. By default we will use approximate MP2-natural orbitals [38, 44] unless stated otherwise (see Appendix A for details). Because we work with plane waves, we shall change the notation from N_g to N_{pw} to be more explicit.

In order to implement the Hamiltonian (III.2) in the quantum circuit with low cost, it is necessary to factorize the Hamiltonian so as to reduce the amount of information needed for the block encoding and to have the smallest possible subnormalization factor. First, we notice that the two-body term in Hamiltonian (III.2) can be expanded into a soft (pseudo) contribution and atomic-centered PAW corrections [39]:

$$(III.5) \quad \kappa_{pqrs} = (\tilde{\rho}_{pq} | \tilde{\rho}_{rs}) + \sum_a^{N_A} \sum_{i_1 i_2 i_3 i_4}^{n_a} C_{i_1 i_2 i_3 i_4}^a D_{pq, i_1 i_2}^{a*} D_{rs, i_3 i_4}^a,$$

respectively, where we introduced the notation for Coulomb matrix elements:

$$(III.6) \quad (f|g) = \iint d^3\mathbf{r} d^3\mathbf{r}' \frac{f^*(\mathbf{r}')g(\mathbf{r})}{|\mathbf{r}' - \mathbf{r}|}.$$

For the definition of $\tilde{\rho}_{pq}$ and other notations we refer the reader to the Appendix B. In order to factorize the first term in Eq. III.5, we employ the plane wave expansion of the Coulomb kernel:

$$(III.7) \quad \frac{1}{|\mathbf{r}|} = \sum_{\mathbf{G}}^{N_{pw}} e^{i\mathbf{G}\mathbf{r}} v(\mathbf{G}).$$

In this expansion, we do not omit the divergent $\mathbf{G} = 0$ component and instead use Wigner-Seitz regularization [45]. For the PAW term, we use eigendecompositions of the tensor $C_{i_1 i_2 i_3 i_4}^a$ and the atomic orbital-pair density matrices, $D_{pq, i_1 i_2}^a$. The resulting Hamiltonian can then be written as follows (see Appendix B for detailed derivation and notations):

$$(III.8) \quad \hat{H} = H^{(0)} + \sum_{p,q}^{N_b} \left(h_{pq} - \frac{1}{2} \sum_r \kappa_{rprq} \right) \hat{E}_{pq} + 2 \sum_{\mathbf{G} \geq 0}^{N_{pw}/2} \sum_{j=1,2} v'(\mathbf{G}) \hat{U}_j(\mathbf{G}) \left(\sum_p^{N_b} f_{p,j}(\mathbf{G}) \hat{E}_{pp} \right)^2 \hat{U}_j^\dagger(\mathbf{G}) + \sum_a^{N_A} \sum_{i_1 \leq i_2}^{n_a} \text{sign}(\epsilon_{i_1 i_2}^a) \hat{U}_{i_1 i_2}^a \left(\sqrt{|\epsilon_{i_1 i_2}^a|} \sum_p^{N_b} f_{p, i_1 i_2}^a \hat{E}_{pp} \right)^2 \hat{U}_{i_1 i_2}^{a\dagger}$$

with $f_{p,j}(\mathbf{G})$ being the eigenvalues of the soft reciprocal orbital-pair density matrix $\eta_{pq,j}(\mathbf{G})$. When the Hamiltonian (III.8) is mapped onto qubits, an additional contribution appears in the one-body term [32, 33]

$$(III.9) \quad h'_{pq} = h_{pq} + \frac{1}{2} \sum_r (2\kappa_{rrpq} - \kappa_{rprq}),$$

and the subnormalization factor in the block encoding becomes

$$(III.10) \quad \lambda = \sum_p^{N_b} |\epsilon_p| + \frac{1}{4} \sum_{j=1,2} \sum_{pq}^{N_b} \xi_{pq}^{(j)} + \frac{1}{2} \sum_a^{N_A} \sum_{i_1 \leq i_2}^{n_a} |\epsilon_{i_1 i_2}^a| \left(\sum_p |f_{p, i_1 i_2}^a| \right)^2,$$

where ϵ_p is the p^{th} eigenvalue of h' [32], and

$$(III.11) \quad \xi_{pq}^{(j)} = \frac{8\pi}{V} \sum_{\mathbf{G} > 0} \frac{1}{\mathbf{G}^2} |f_{p,j}(\mathbf{G})| |f_{q,j}(\mathbf{G})| = \iint_V d^3\mathbf{r} d^3\mathbf{r}' \frac{f'_{p,j}(\mathbf{r}) f'_{q,j}(\mathbf{r}')}{|\mathbf{r} - \mathbf{r}'|} = (f'_{p,j} | f'_{q,j}).$$

This factorization is of double factorization form [32, 46] apart from the fact that there is an additional sign in the PAW contribution, $\text{sign}(\epsilon_{i_1 i_2}^a)$. This is because $C_{i_1 i_2 i_3 i_4}^a$ is not positive definite and the standard Cholesky decomposition could not be used. Instead, we have used a conventional eigendecomposition. In the next Section IV, we outline the modifications to a quantum circuit from Ref. [33] in order to take the two-body PAW term into account.

IV. BLOCK ENCODING

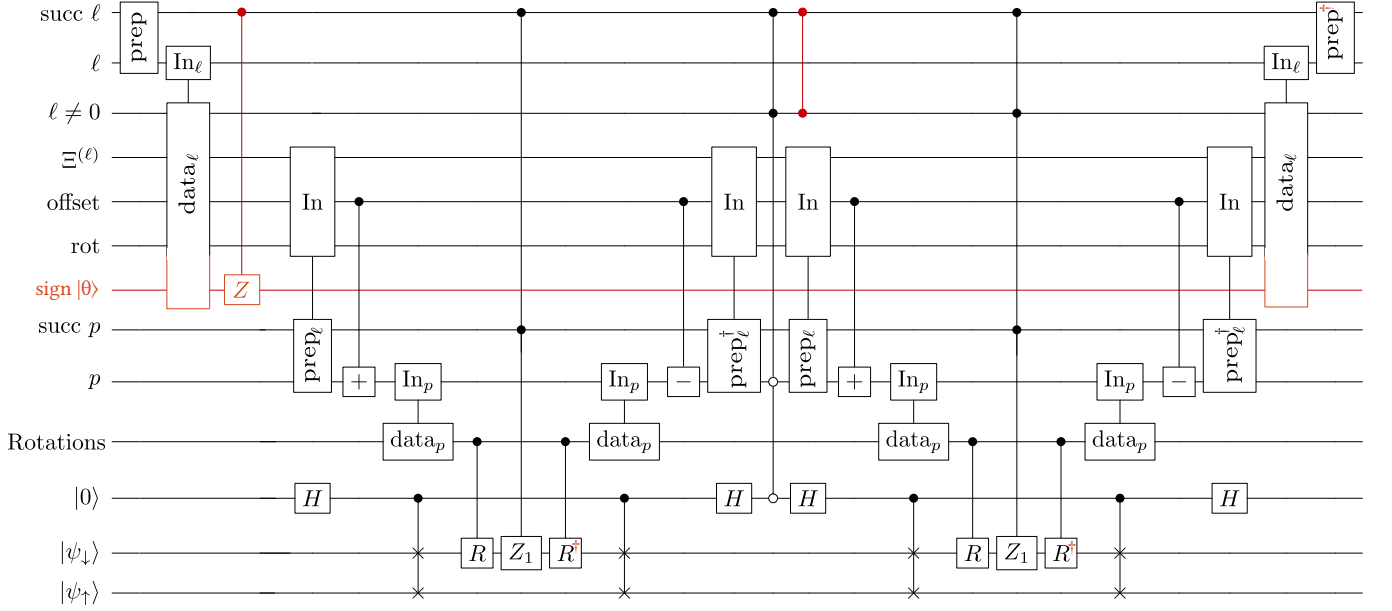


FIG. 2. Circuit for the block encoding of the double factorised UPAW Hamiltonian. Our modifications in red enable the signs required by the UPAW contribution to the interaction term. The image is a modified version of Fig. 16 in [33].

Our block encoding of the UPAW Hamiltonian closely follows double factorization [32] as presented in the appendix C of [33]. Figure 2 shows the block encoding circuit of [33] along with our modifications in red. First, the one-body term and factorised terms in the Hamiltonian (III.8) are indexed by $\ell = 0, 1, \dots, L$. While $\ell = 0$ flags the one-body terms, positive values of ℓ flag the various factorised two-body terms indexed by $\mathbf{G}, j, a, i_1, i_2$ in (III.8). Counting those terms results in

$$(IV.1) \quad L = N_{\text{pw}} + \sum_a^{N_A} n_a(n_a + 1)/2.$$

The key difference of the UPAW Hamiltonian compared to the prior work is the coefficients $\text{sign}(\epsilon_{i_1, i_2}^a)$ in the UPAW contribution, Eq. (B.25), to the interaction term. These signs cannot be absorbed into a square with real coefficients and therefore must be treated separately. This is achieved by our main modification to the circuit as shown in Fig. 2: The signs are loaded into an additional ancilla $|\theta\rangle$ (with $|0\rangle$ indicating $+$ and $|1\rangle$ indicating $-$) during the data loading indexed by the ℓ register. We use $\text{sign}(\epsilon_{i_1, i_2}^a)$ for the UPAW contribution (B.25) to the interaction term and $+1$ for all other terms. The phase corresponding to the sign is then implemented by acting on this ancilla with a Z gate, conditioned on the success of the state preparation over ℓ . We also add the complex conjugation to the uncomputation of the R rotations that were missing in the original circuit. The square from the factorization is implemented by performing the inner block encoding (of the base of the square) twice in the case of two-body terms $\ell \neq 0$, with an intermediate reflection, to which we have added a CZ to correctly recover the second Chebyshev polynomial, see Appendix E.

This extension of the double factorization circuit to implement UPAW only incurs a negligible increase in fault-tolerant resources: Firstly, the output register of the unary iteration over ℓ needs one additional qubit to store the sign of the interaction terms. The increased register size also leads to a slight additive increase in Toffoli cost for implementing the QROAM for the data loading indexed on ℓ . As the CZ implementing the sign is a Clifford gate, it does not contribute to the fault-tolerant resource cost (see Appendix C describing the error correction scheme). Following the convention in Appendix C of [33], where costing of the double factorisation algorithm is re-presented, this amounts to increasing their Eqn. C29 for b_o by one. In the OpenFermion [47] package's implementation of the double factorisation costing, this modification can be readily achieved by increasing the b_o variable by one.

V. RESULTS

A. Space and Time Complexity of the Quantum Algorithm

In this section, we present the asymptotic complexity of the algorithm in the worst-case scenario, when only terms in the Hamiltonian with absolute value less than 10^{-10} are neglected. Such a small truncation provides results well within chemical accuracy. The total Toffoli count of qubitized QPE is $O(\sqrt{\Gamma}\lambda/\epsilon_{\text{QPE}})$, with $O(\sqrt{\Gamma})$ qubits [30, 31]. The subnormalisation (one-norm) λ and target QPE error ϵ_{QPE} give the number of iterations of the block encoding required. The cost of the block encoding is dominated by a QROAM circuit loading data of total size Γ . Here, the main contribution to the data that must be loaded to implement the Hamiltonian is the L rotations (see Eq. IV.1) for the two-body terms of dimensions $N_b \times N_b$. Each rotation angle is specified with \beth bits, resulting in total data size $\Gamma = LN_b^2 \beth$, like in double-factorization [32]. Specifically, for our LN_b data items of size $N_b \beth$ each (rotations are loaded column-by-column), the QROAM allows a space-time tradeoff

$$(V.1) \quad \text{QROAM Toffolis: } \left\lceil \frac{LN_b}{k_r} \right\rceil + N_b \beth (k_r - 1) \quad \text{QROAM qubits: } N_b \beth k_r + \left\lceil \log \frac{LN_b}{k_r} \right\rceil$$

with a tunable parameter k_r (which must be a power of 2). When it is chosen to minimise Toffoli count, we recover Toffoli and qubit cost $O(\sqrt{\Gamma})$ for the block encoding.

In practice, we have the scaling $\Gamma = O(N_{\text{pw}} N_b^2)$, because $N_{\text{pw}} \gg N_A$, and \beth can be omitted as it only weakly depends on the size of the system and in this work we kept it constant ($\beth = 20$) as will be discussed in Section VB. For the subnormalisation, one can expect that $\lambda = O(N_b^2)$, by using the assumptions $\xi_{pq}^{(j)} = O(1)$ in Eq. (III.10) and that the last term in the equation is small (as verified numerically). We will further analyse the complexity of the algorithm in two regimes, the continuum limit and the thermodynamic limit.

The first regime we consider is the continuum limit, in which system size N_A is fixed, and the number of bands $N_b \rightarrow \infty$ increases. While at first glance this requires $N_{\text{pw}} = O(N_b)$, in practical calculations, N_{pw} is always significantly larger than N_b , especially for molecules due to the large simulation box needed to reduce the interaction between periodic images. For any practical calculation when natural orbitals are employed, the correlation energy converges for $N_b \ll N_{\text{pw}}$ [38] such that N_{pw} can be taken as a large, fixed constant. Consequently, we expect $\Gamma = O(N_b^2)$ and total Toffoli complexity $O(N_b \lambda)$ and space complexity $O(N_b)$ for the convergence of correlation energy w.r.t the continuum limit. This indicates that the qubit complexity would scale only linearly in the number of orbitals, until it reaches the plane-wave basis set size.

We verify this scaling numerically with a test system of four hydrogen atoms arranged in a square with length 2 Bohr, see Fig 3(a,c). Since the two-body term is the dominant contribution in the asymptotic regime, we considered only its contribution to the one-norm:

$$(V.2) \quad \lambda_2 = \frac{1}{4} \sum_{j=1,2} \sum_{pq}^{N_b} \xi_{pq}^{(j)} + \frac{1}{2} \sum_a^{N_A} \sum_{i_1 \leq i_2}^{n_a} |\epsilon_{i_1 i_2}^a| \left(\sum_p |f_{p, i_1 i_2}^a| \right)^2.$$

For the molecular hydrogen, we used a $10 \times 10 \times 10 \text{ \AA}^3$ box and the kinetic energy cutoff was set to 800 eV. As in Ref. [33], we considered varying numbers of orbitals from 10 to 100. The results in Fig. 3(c) show that Γ scales almost quadratically $\Gamma = O(N_b^{1.93})$, and Fig. 3(a) shows that the subnormalization scales as $\lambda = O(N_b^{2.15})$, both close to the theoretical scalings discussed above.

The second regime we consider is the thermodynamic limit, in which supercell size and number of atoms $N_A \rightarrow \infty$ increases, and the number of bands per atom $n_b = N_b/N_A$ is fixed. The number of plane waves must also increase linearly with the number of atoms, $N_{\text{pw}} = O(N_A)$. Consequently, we expect $\Gamma = O(N_A^3)$ and total Toffoli complexity $O(N_A^{1.5} \lambda)$ and space complexity $O(N_A^{1.5})$. Again, we check this scaling numerically. To that end, we consider crystalline diamond with supercells of 2–128 atoms with a fixed number of orbitals per atoms (4 natural orbitals per atom). We use a kinetic energy cutoff of 600 eV. The results are presented in Fig. 3(b, d). We see that the one-norm also scales almost quadratically $O(N_A^{2.08})$, and $\Gamma = O(N_A^{2.97})$, close to the theoretical scalings discussed above. The asymptotic results in this regime are summarized in Table I, where for comparison we also provide asymptotic scalings of other factorization techniques.

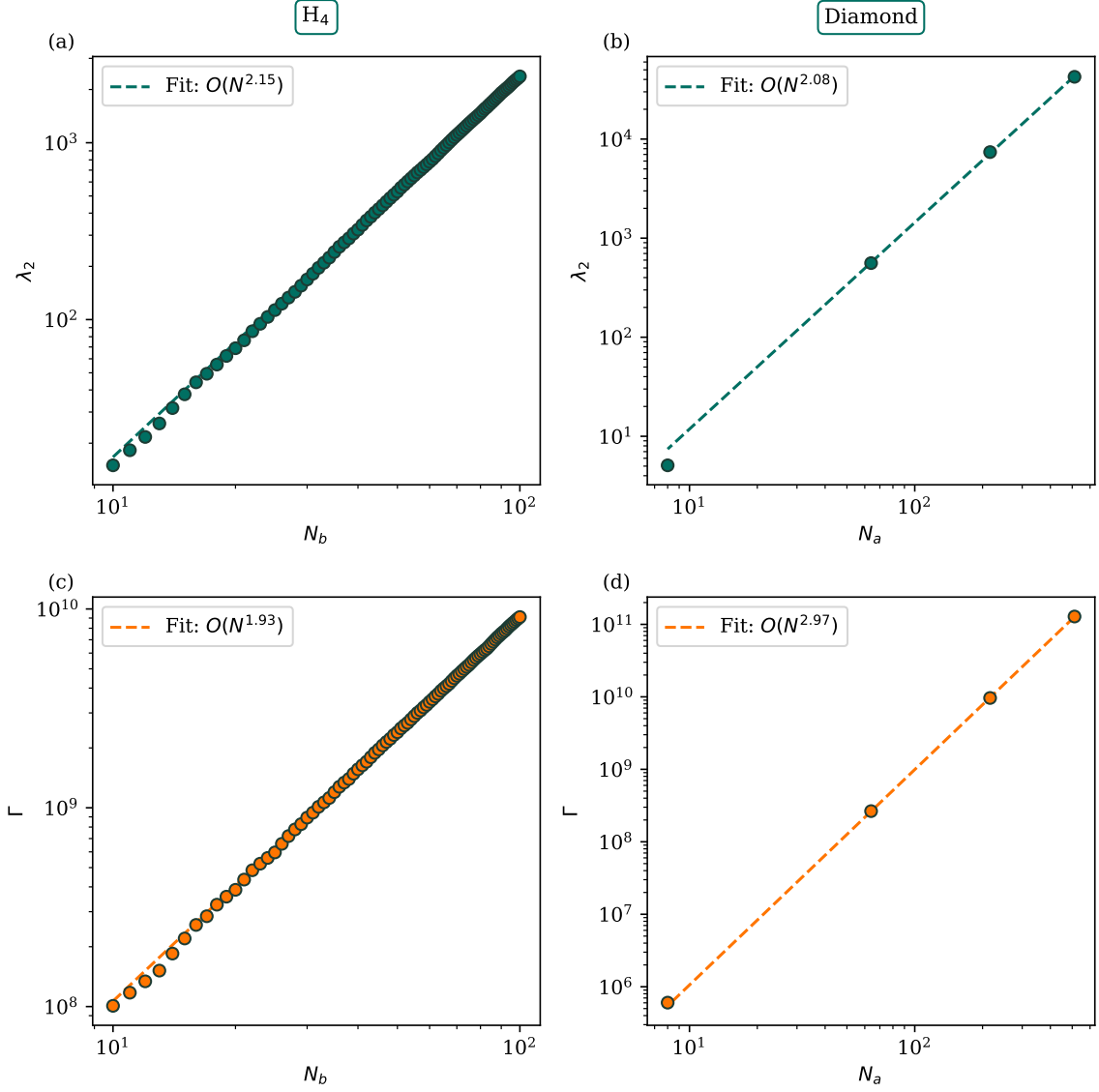


FIG. 3. **Scaling of different parameters that determine the efficiency of the quantum algorithm.** (a, b) The subnormalization factor λ_2 in the block-encoding due to the two-body term. (c, d) The amount of information needed to specify the Hamiltonian's linear-combination-of-unitaries decomposition, Γ . Only parameters with absolute value larger than 10^{-10} are counted as being non-zero. For the H_4 example (a, c), the number of atoms and plane waves is fixed and only the number of orbitals is changed while for Diamond (b, d) the number of atoms is changed which in turn also changes the total number of orbitals and plane waves.

Factorization	Qubit Complexity	Toffoli Complexity
Sparse [31]	$N_A + \sqrt{S}$	$(N_A + \sqrt{S})\lambda_{\text{Sparse}}/\epsilon$
SF [31]	$N_A^{3/2}$	$N_A^{3/2}\lambda_{\text{SF}}/\epsilon$
DF [32]	$N_A\sqrt{\Xi}$	$N_A\sqrt{\Xi}\lambda_{\text{DF}}/\epsilon$
THC [33]	N_A	$N_A\lambda_{\text{THC}}/\epsilon$
PW-PAW [This work]	$N_b\sqrt{N_{\text{pw}}} \propto N_A^{3/2}$	$N_A^{3/2}\lambda_2/\epsilon$

TABLE I. Asymptotic complexities of different factorization algorithms for 3D periodic systems w.r.t. the number of atoms (system size) N_A , and a fixed number of orbitals per atom, in second quantization. N_b is the number of bands (orbitals) and N_{pw} is the number of plane waves. For Sparse, Single Factorization (SF) and Double Factorization (DF), one can obtain a further polynomial asymptotic improvements in qubit and Toffoli counts by using Wannier or Bloch functions (see Ref. [34] for Sparse algorithm with Wannier and Bloch functions, Ref. [35] for Sparse algorithm and other factorizations with Bloch functions) if the system possesses translational symmetry. For the Sparse approach, $S = O(N_A^4)$ and for Double Factorization, $\Xi = O(N_A)$ in the worst case scenario. Analytical and numerical results suggest that, $\lambda_2 = O(N_b^x) = O(N_A^x)$, with $2 \leq x < 2.5$.

B. Quantum Resource Estimates

In order to estimate the energy within a given error, one has to account for the different approximations used in both the quantum algorithm and Hamiltonian approximations. The total error in the single point calculations (one estimation of the energy for a given position of nuclei) can be decomposed in a sum of the following errors:

$$(V.3) \quad \epsilon_{\text{tot}} = \epsilon_{\text{QPE}} + \epsilon_{\text{trunc}} + \epsilon_{\text{BE}} + \epsilon_{\text{orb}} + \epsilon_{\text{pw}} + \epsilon_{\text{paw}},$$

where ϵ_{QPE} is error from the QPE measurement, ϵ_{trunc} is the error due to the truncation of the Hamiltonian matrix elements, ϵ_{BE} is the error incurred when constructing the block encoding, ϵ_{orb} is the error due to the finite number of orbitals (the number of natural orbitals, N_b), ϵ_{pw} is the error due to the finite size of the plane wave basis, and ϵ_{paw} is the error due to the PAW approximation. ϵ_{BE} is affected by the bitlengths of various parameters used in the circuit: The parameters \aleph for the bitlength of keep probabilities affect the error in amplitudes from coherent alias sampling, and the parameters \beth affects the error in the rotations [33]. Usually ϵ_{BE} is negligible compared to the other errors; consistent with the OpenFermion [47] implementation of double factorisation costing as in [33], we simply use the values $\aleph = 10$ and $\beth = 20$ throughout. Below, we will analyze the other errors and provide the resource estimates for crystalline solids and the defect states.

1. Crystalline solids

In this section, we present the quantum resource requirements for estimation of the ground state energy of crystalline solids without defects. Our goal is to estimate the energy per cell consisting of many atoms and using large basis sets. In order to estimate such an energy at the large basis set limit, we use the down-sampling method. While this method is usually applied w.r.t to k -point sampling, it also can be applied with respect to supercell size and, in fact, when the k -point mesh is Γ -centred both approaches are equivalent. To estimate the energy per cell using a $[n+1, n+1, n+1]$ supercell, one can estimate the converged energy per cell for $[n, n, n]$ and add the energy difference between $[n+1, n+1, n+1]$ and $[n, n, n]$ for a fixed number of bands. Let $E(n, n_b)$ denote the ground state energy estimated using a $[n, n, n]$ supercell with $n_b = N_b/N_A$ bands per atom. Then the down-sampling energy is

$$(V.4) \quad E_{\text{ds}}(n+1) = E_{\text{ds}}(n) + E(n+1, n_b) - E(n, n_b),$$

We apply this equation up to $n = 3$ which results in:

$$(V.5) \quad \begin{aligned} E_{\text{ds}}(1) &= E(1, n_b'') \\ E_{\text{ds}}(2) &= E_{\text{ds}}(1) + E(2, n_b') - E(1, n_b') = E(1, n_b'') + E(2, n_b') - E(1, n_b') \\ E_{\text{ds}}(3) &= E_{\text{ds}}(2) + E(3, n_b) - E(2, n_b) = E(1, n_b'') + E(2, n_b') - E(1, n_b') + E(3, n_b) - E(2, n_b), \end{aligned}$$

where the three parameters can be chosen $n_b < n_b' < n_b''$ to control the number of orbitals per atom and the error in the energy, ϵ_{orb} . Therefore, one would have to run 5 QPE calculations and the total error for $E_{\text{ds}}(3)$ would be a sum of 5 errors from each single point calculations.

To reduce the amount of classical data from QROAM, it is a common practice to truncate the small values of the parameters which determine the Hamiltonian elements [32, 33] and this affects ϵ_{trunc} . The most dominant cost is

due to the plane wave expansion of the Coulomb kernel and the factorization of the orbital-pair density matrices. Therefore, we truncate the inner rank of the plane-wave decomposed two-body term, namely, we set $f_{p,j}(\mathbf{G})$ to zero if

$$(V.6) \quad |f_{p,j}(\mathbf{G})| \leq \delta |\mathbf{G}|,$$

where δ is a small number. Therefore, ϵ_{trunc} depends on δ , and so $\epsilon_{\text{trunc}} = \epsilon_{\text{trunc}}(\delta)$. Below, we will identify all error parameters and we start with quality of UPAW setups and plane wave basis, ϵ_{paw} and ϵ_{pw} .

In order to estimate the last two errors, ϵ_{pw} and ϵ_{paw} , we will use density functional theory where we can compare the result of our calculations to both the high-quality all-electron calculations for solids (Δ -DFT data set) [18, 48, 49] as well as simple diatomic molecules. To generate all-electron binding curves for molecules, we used the uncontracted ANO-RCC-VQZP Gaussian basis set [50], readily available from Basis Set Exchange [51–53], and scalar relativistic corrections as implemented in PySCF [54–56]. We consider PAW setups which are available in GPAW [36, 57, 58], as well as new UPAW setups, norm-conserving Vanderbilt pseudopotentials [40, 59] and HGH pseudopotentials (a relativistic version of GTH) [20, 21, 60]. Results on norm-conserving pseudopotentials for Δ -DFT data are readily available from Ref. [48] and [15, 61]. All plane-wave basis set calculations have been carried out with GPAW [36, 57, 58] and when we simulated solids we have used a dense Monkhorst-Pack k-point grid [62] (16 points/ \AA^{-1}).

Fig. 4 shows the results of these calculations. Fig. 4(a) shows the binding curves obtained at 600 eV with UPAW and PAW setups. As can be seen the error in the binding energy is well within chemical accuracy. 600 eV corresponds to practically converged results as shown in Figure 4(c). The PAW method demonstrates slightly faster convergence (around 400 eV) as expected. Fig. 4(b) shows the equation of states of graphite calculated with different methods at the small value of 600 eV, and Fig. 4(d) demonstrates the convergence of error w.r.t all-electron calculations towards the limit of 2500 eV. The lower the curve on that graph the closer the result to the converged value. The converged values with UPAW and PAW can be achieved already at 600 eV while norm-conserving pseudopotentials require a higher plane-wave cutoff. While HGH pseudopotential demonstrates good accuracy for this material, it requires the largest plane wave cutoff among all methods. For example, to reach an accuracy of 1.0 meV/atom one has to use more than 1000 eV kinetic-energy cutoff and for an accuracy of 0.1 meV/atom, one has to use even higher a 1500-2000 eV cutoff. We also note that we do not guarantee that 2500 eV corresponds to absolute convergence, but higher plane wave cutoffs are too computationally expensive to use in any practical calculations. As can be seen, the error introduced due to the (U)PAW approximation and finite PW basis set is small, -0.12 meV/atom \approx 0.044 mHa/atom, and in the following resource estimations we will use a kinetic-energy cutoff of 600 eV. In order to show that the UPAW approach is transferable to other more challenging elements such as transition metals, we present the results for a few other elements based on the Δ -DFT data in the Table II. As one can see, the norm-conserving pseudopotentials exhibit large errors for elements such as Cr and Mn, while the PAW-based methodology provides a small error. A particularly difficult system is Cr bulk where the inclusion of semicore electrons is necessary in UPAW setups in order to obtain accurate results. However, UPAW setups with a small number of electrons (6 valence electrons) for Cr is comparable in accuracy with norm-conserving pseudopotentials where semicore electrons are included. We note, however, that it is probably possible to refit the norm-conserving pseudopotentials to minimize this error.

To choose the number of orbitals per atom, n_b, n'_b, n''_b , as well as the truncation threshold δ , the MP2 correlation energy is calculated for different numbers of orbitals until convergence is reached up to the desired accuracy. Fig. 5 and Table III show results of such calculations using both a standard supercell approach and down-sampling method. As is expected, the down-sampling approach converges much faster than the supercell approach and reaches chemical accuracy already at 13 orbitals/atom. We then carry out calculations with n''_b and different values of n'_b, n_b and δ to find allowable error parameters within the error budget. We find that with $\delta = 3 \cdot 10^{-5}$ and $n'_b = 26$, we stay within chemical accuracy for $n_b \geq 17$, and the error is 0.96 mHa. Consequently, we have to estimate the quantum resources for running QPE with 5 sets of parameters as presented in Table IV. For each set, we estimate the quantum resources with QPE accuracy of the remaining error budget, $\epsilon_{\text{QPE}} = (1.60 - 0.96 - 0.44)/5 \approx 0.04$ mHa. The value of 0.44 corresponds to estimation from UPAW and finite plane-wave basis set as was described above. As can be seen the most computationally demanding calculations are for the largest system with a 54 atom cell and 17 orbitals per atom. This requires around 140,000 logical qubits and a number of Toffolis on the order of 10^{14} . We note that even smaller calculations with 2 atoms in the cell and 160 orbitals/atoms require large quantum resources, \approx 13,000 logical qubits and on the order of 10^{13} Toffolis. Assuming that this computation will be run on a superconducting device with nearest-neighbour connectivity on a square lattice with a physical error rate of 0.01%, we estimate that such calculations would require around 23.8 million and 316 million physical qubits for 2 atoms cell with 80 orbitals per atom and 54 atom cell with 17 orbitals per atom, respectively. This estimation assumes surface code error correction (See Appendix C for more details).

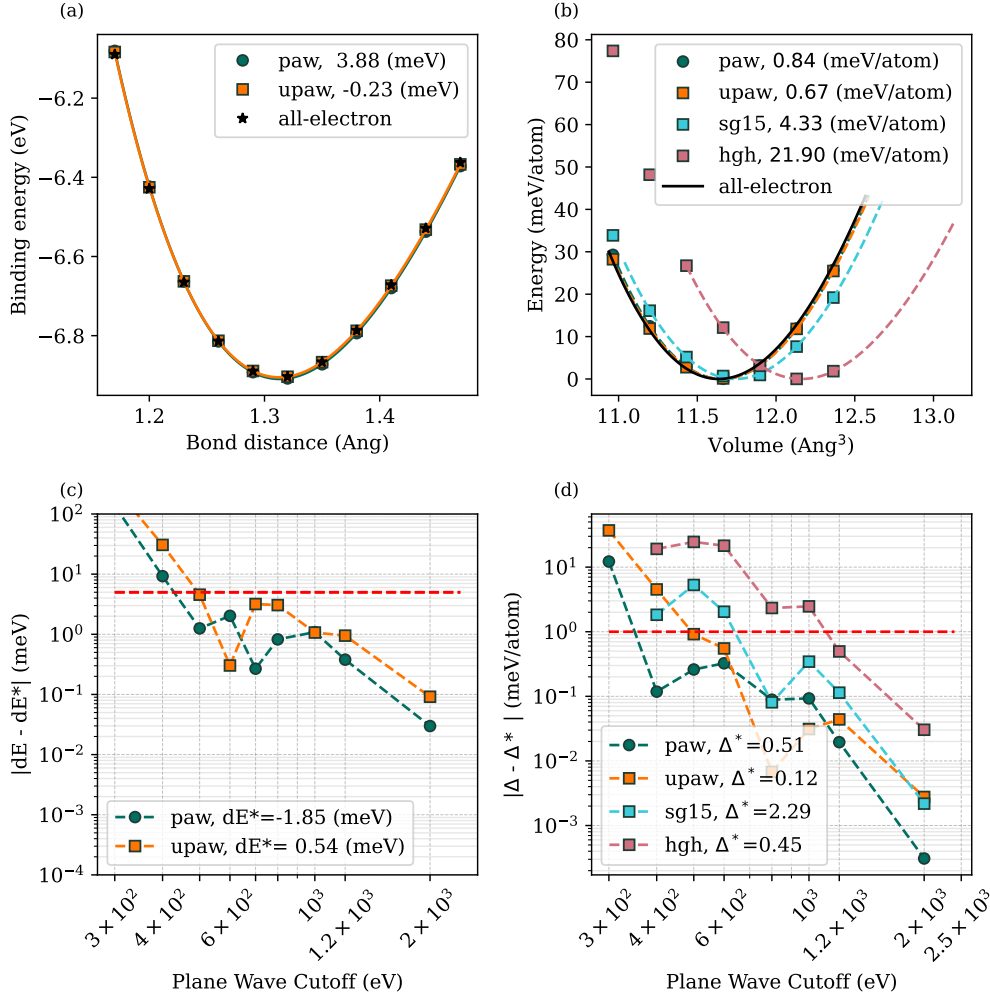


FIG. 4. **Accuracy of norm-conserving pseudopotential and PAW approaches for Carbon.** (a) C₂ binding curve calculated with all-electron approach using Gaussian type orbitals and (U)PAW setups with plane waves. The kinetic energy cutoff is 600 eV. Labels also indicate the binding energy error w.r.t. to all-electron calculations. (b) Equation of state of graphite calculated with norm-conserving pseudopotential (SG15 [40, 59]), PAW and UPAW setups at 600 eV plane-wave cutoff. All-electron data is from Δ -DFT data set [18, 48, 49]. Labels also indicate the error, Δ , w.r.t. to all-electron calculations. Δ is defined as the root-mean-square energy difference between the equations of states obtained with all-electron calculations and pseudopotentials/(U)PAW approaches. (c) Convergence of binding energy error towards the high-plane wave cutoff limit of 2500 eV. The red dotted line corresponds to an error of 5 meV (0.18 mHa). (d) Convergence of error, Δ , towards the high-plane wave cutoff of 2500 eV. The red dotted line corresponds to an error bar of 1.0 meV/atom. The lower the curve the closer the result to the converged values.

2. Defects in Solids. Nitrogen-Vacancy Centre in Diamond.

Our methodology can be applied to materials with defects. Typical calculations of defects are performed in the supercell approach without k-point sampling, and the size of the supercell should be large enough so as to reduce the interaction between periodic images of the defect state. Here we estimate the resources for energy state estimation using the supercell approach.

Quantum defects in semiconductors are of great interest as they can be utilized in a range of applications such as sensing [63–66], quantum communication [67–69] and computation [70–74]. A negatively charged Nitrogen-Vacancy (NV⁻) centre in diamond is one of the most studied and understood defects. However, predicting the excitation energy levels using electronic structure methods is challenging due to large supercells required to reduce the interaction of the centre with its periodic images (the length-scale problem) as well as the multi-determinantal nature of singlet excited states. Fig. 6 shows energy levels of the excited triplet ³E and two singlet states, ¹E and ¹A₁, obtained with different electronic structure methodologies [75–81]. The most challenging state is the singlet ¹A₁ state and as

Element	UPAW	PAW	SG15 [61]	HGH [48]
O	0.55	0.17	0.39	1.30
Cr	0.47 (12.6)	3.10	20.82	13.68
Mn	0.67 (2.85)	1.01	13.05	15.68
Ni	0.54 (0.18)	4.51	2.16	1.38

TABLE II. **The error, Δ , w.r.t. to all-electron calculations [18, 48, 49].** Δ is defined as the root-mean-square energy difference between the equations of states obtained with all-electron calculations and a tested approach. Values are in the units of meV/atom. Values in parentheses are obtained from setups with only valence electrons (6, 7, 10 electrons for Cr, Mn and Ni, respectively). All other calculations include semicore electrons explicitly.

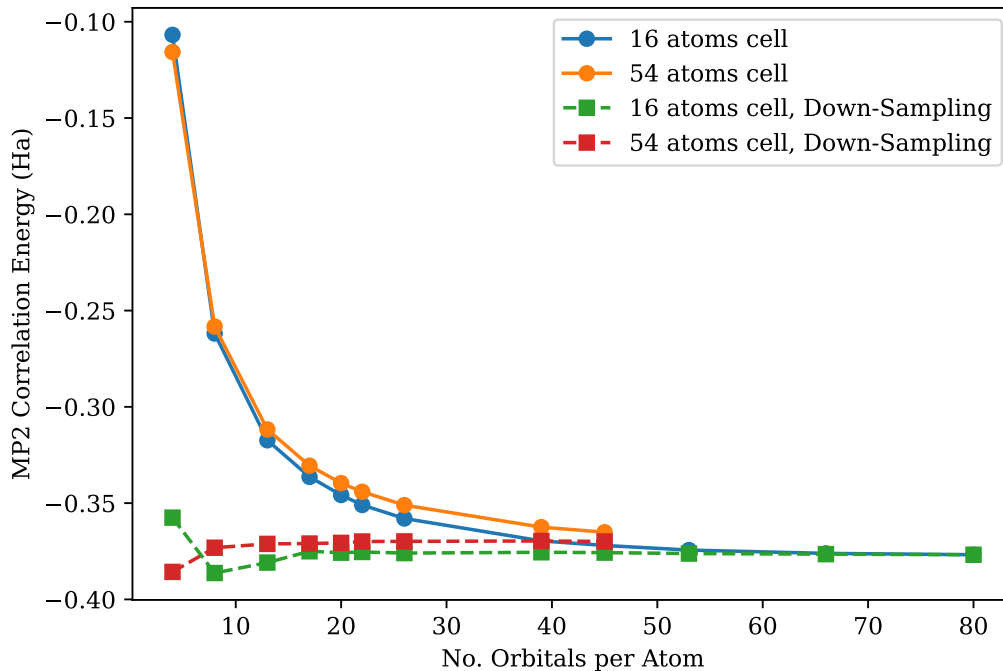


FIG. 5. **Convergence of MP2 correlation energy per cell (2 atoms) of diamond with respect to the number of orbitals per atom.** Calculations are presented for both the down-sampling method and the supercell approach (16 and 54 atoms cells).

one can see the prediction of its energy ranges from 1.1 eV (GW-BSE calculations [78]) up to 2.1 eV (Diffusion Monte Carlo calculations [79]). Given such a large scattering of the data as given by mean-field approaches, many-body perturbation theory, quantum embedding and wavefunction methods, it is clear that having an additional more reliable method to predict the energetics of such a system would be very beneficial. We note that such and similar systems have been explored using quantum embedding methods in the context of quantum computation [77, 82]. However, the quantum embedding methods used there rely on many approximations such as an exchange-correlation functional, the way in which the double-counting term is implemented, and the level of theory used for calculation of the screened Coulomb interaction [83]. These approximations introduce uncontrollable errors in the calculations and results can then be verified only after the comparison with experimental data is made. Calculations in the supercell approach without additional approximations would be more predictive.

Fig. 6 shows the quantum resource requirements for the energy estimation of this system on an error-corrected quantum computer. In the calculations, we used 4, 8, 13, 17 and 20 natural orbitals per atom. Since we do not carry out the error analysis due to truncation using MP2 theory (because of the degenerate homo-lumo gap), we choose the conservative truncation parameter $\delta = 3 \cdot 10^{-6}$ – an order of magnitude lower than in previous section. The QPE error budget is 1.0 mHa per supercell. We have used a 600 eV kinetic-energy cutoff and UPAW setups as described before. Fig. 6 shows that even the smallest instances of such simulations would require around 80,000 logical qubits and the number of Toffolis is around $7.3 \cdot 10^{12}$. With the increase of the number of orbitals, the number of logical qubits grows only linearly and the Toffoli count, which would be proportional to the total runtime, scales polynomially as $O(N_b^{3.4})$.

Orbitals per Atom	ϵ_{orb}	$\epsilon_{\text{orb}} + \epsilon_{\text{trunc}}(\delta = 3 \cdot 10^{-5})$
n_b	$(n_b'', n_b') = (80, 80)$	$(n_b'', n_b') = (80, 26)$
4	15.80	16.93
8	3.25	3.87
13	1.25	2.40
17	1.08	0.96
20	0.72	0.17
22	0.02	-0.60
26	-0.04	-0.70

TABLE III. **Error due to the finite size of the orbital basis set and truncation.** Deviation of the MP2 correlation energy from an accurate value estimated using down-sampling technique with $n_b = 45$ orbitals per atom and a (3, 3, 3) supercell with $n_b'' = n_b' = 80$. The last column presents the deviation for a finite truncation and for $n_b'' = 80$ and $n_b' = 26$. Energy is given in mHa/primitive cell (2 atoms).

Size of the cell (n, n, n)	Orbitals per Atom	Logical Qubits	Toffolis
(1, 1, 1)	$n_b'' = 80$	13313	$7.33 \cdot 10^{13}$
(1, 1, 1)	$n_b' = 26$	4443	$2.51 \cdot 10^{12}$
(2, 2, 2)	$n_b' = 26$	67593	$1.85 \cdot 10^{14}$
(2, 2, 2)	$n_b = 17$	44262	$4.41 \cdot 10^{13}$
(3, 3, 3)	$n_b = 17$	148937	$5.23 \cdot 10^{14}$

TABLE IV. **Quantum resource estimates for diamond.** The QPE error budget is 0.04 mHa/primitive cell.

VI. DISCUSSION AND CONCLUSION

We have introduced the unitary projector augmented-wave method and used it with a plane-wave basis set to derive an efficient representation of Hamiltonians suitable for quantum computation of materials. We have analysed the resource requirements of this approach for high-accuracy calculations. While there have been recent developments in quantum computing methods for materials calculations using norm-conserving pseudopotentials and Gaussian basis sets [34, 35], it is somewhat hard to compare the approaches because the comparison of quantum resources should be made for the same accuracy of calculations. To achieve this, one would need to carry out all-electron correlated calculations of materials at scale and converged basis set limits and produce reliable reference values. Such benchmarks are available for density functional theory [15, 18, 19] but we are not aware of any for wavefunction calculations. Such simulations would require enormous CPU time and we did not attempt to carry out this comparison in this work. However, if we take a number of natural orbitals in our calculations that corresponds to the size of the cc-pVDZ basis set (13 orbitals per atom) for diamond and estimate the quantum resources with a QPE error budget of 1.6 mHa/cell, we obtain $4.0 \cdot 10^{11}$ Toffolis and 33878 logical qubits, which is similar to the value obtained using tensor-hyper contraction in Ref. [35] ($4.85 \cdot 10^{11}$ Toffolis and 36393 logical qubits). We note that using Bloch functions with k-point sampling and primitive cell instead of supercell calculations [34, 35] can provide a polynomial speed up for crystalline solids. However, this does not bring any advantage for other applications such as defects states where calculations must be carried out in the supercell so as to minimize the interaction between periodic images. For this reason, we did not explore Bloch or Wannier functions in this work.

We have also presented a strongly correlated system, the negatively charged nitrogen-vacancy defect in diamond, where classical algorithms provide scattered results for the energy of the excited states. While the quantum computing algorithms require resources that scale polynomially with system size, significant advances must be made to reduce the quantum resources further to a feasible size for realistic fault-tolerant quantum computers. Only then could one potentially use such algorithms for accurate *ab initio* calculations of the defect states. There are promising avenues for reducing the costs, by considering the electronic structure problem in first quantization instead of second quantization. Interesting works on incorporating pseudopotentials in first quantization have recently been published [23, 24]. The PAW method quite often requires the smaller number of plane wave coefficients and demonstrates a higher accuracy as indicated in density functional theory calculations [15, 18, 19, 48], especially for transition metals as is shown in the Table II. Therefore, it will be beneficial to also implement the PAW approach within first quantization. Unlike pseudopotentials, the PAW approach also modifies the two-body term and in order to incorporate this, non-trivial modifications to the method presented in Refs [22, 24, 84] might be required. One simple way to incorporate the PAW method is to use the first quantization approach developed in Ref. [85], which loads the electronic integrals from QROAM, unlike the approach of Refs [22, 84]. By additionally employing basis sets that diagonalize the two-body term, such as dual plane waves [10], such an approach might provide a viable path to

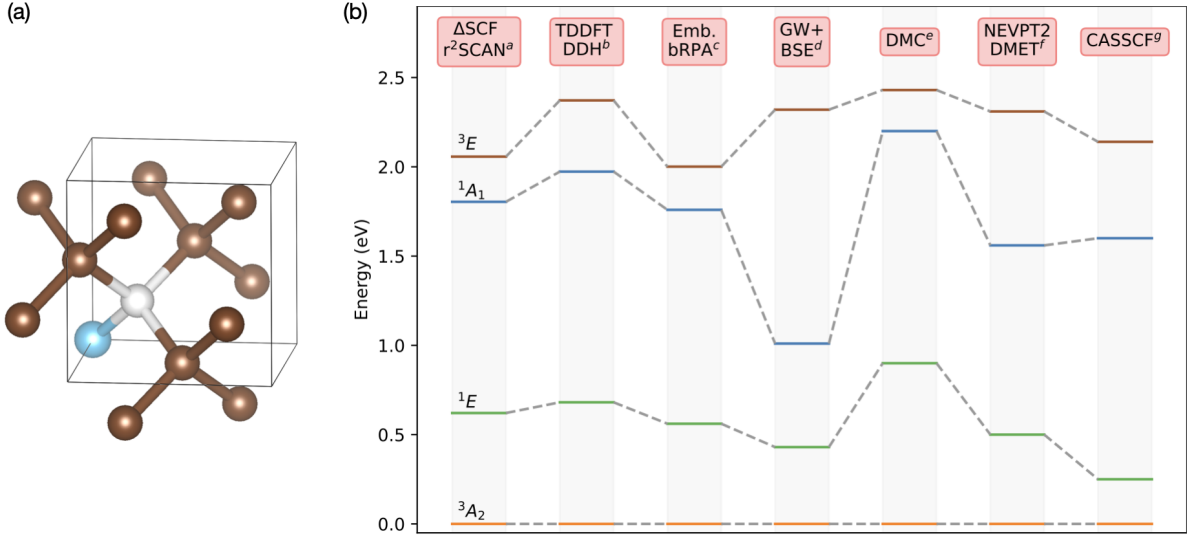


FIG. 6. **Nitrogen-vacancy centre in diamond and excitation energies** (a) Schematic representation of the centre. Carbon atoms are brown, Nitrogen is blue, and the vacancy is white (b) Excitation energy of the negatively-charged NV centre calculated using different classical algorithms. ^aRef.[75], ^bRef.[76], ^cRef.[77], ^dRef.[78], ^eRef.[79], ^fRef.[80], ^gRef.[81]

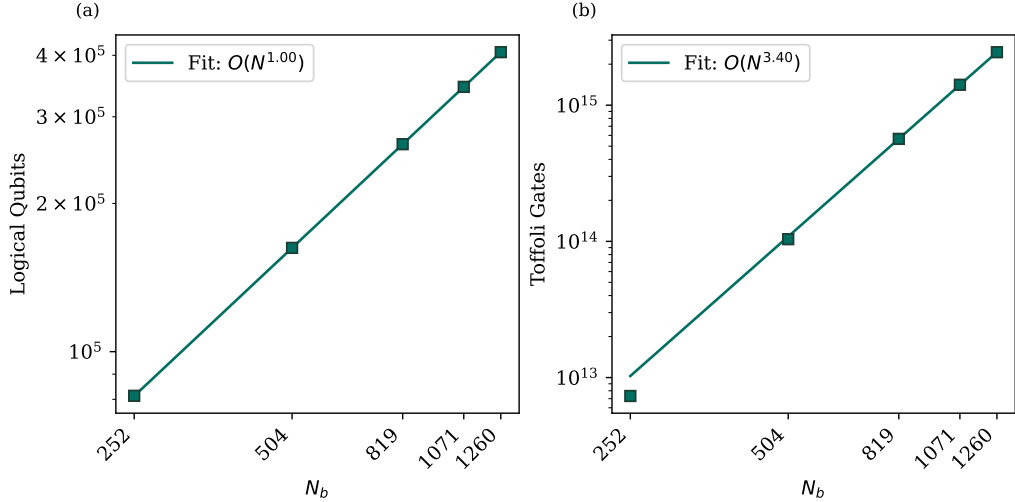


FIG. 7. **The number of logical qubits (a) and Toffoli gates (b) vs. the number of orbitals required for QPE computation of the ground state of NV⁻ centre in diamond.** Calculations have been carried out for a 63 atom supercell and the QPE error budget is 1.0 mHa.

significant reduction of quantum resources.

VII. ACKNOWLEDGEMENT

We thank Nick Blunt for discussions, carefully reading the manuscript and providing valuable suggestions. The work presented in this paper was part funded by a grant from Innovate UK under the 'Feasibility Studies in Quantum Computing Applications' competition (Project Number 10074148). M.B. is a Sustaining Innovation Postdoctoral Research Associate at Astex Pharmaceuticals and thanks Astex Pharmaceuticals for funding, as well as his Astex colleague Patrick Schoepf for his support.

Appendix A: Compression of virtual space with approximate MP2-natural orbitals

In order to reduce the size of the virtual space, we use approximate MP2 natural orbitals [38, 44]. These orbitals allow for much faster convergence to the full basis set limit compared to canonical KS or HF orbitals. By definition, these orbitals diagonalize the approximate-MP2 density matrix [44]:

$$(A.1) \quad D_{ab} = \sum_{c \in \text{virt}} \sum_{i \in \text{occ}} \frac{\kappa_{icbi} \kappa_{icai}^*}{(\epsilon_b + \epsilon_c - 2\epsilon_i)(\epsilon_a + \epsilon_c - 2\epsilon_i)},$$

where N_{occ} is the number of occupied canonical orbitals, N_{virt} is the number of virtual canonical orbitals, $\epsilon_{i/a/b/c}$ are eigenvalues of HF states. This matrix can be calculated using $O(N_{\text{pw}}N_{\text{occ}}N_{\text{virt}}^2)$ operations and $O(N_{\text{pw}}N_{\text{occ}}N_{\text{virt}})$ memory in the plane-wave basis set. In the first step, N_{virt} is chosen as large as possible ($N_{\text{occ}} + N_{\text{virt}} = N_{\text{pw}}$). Assuming natural orbitals are ordered according to eigenvalues of the approximate MP2 density matrix, we then choose first several natural orbitals (the exact number for each specific case described in the text) as virtual orbitals for subsequent calculations.

Appendix B: Matrix elements in PAW formalism and plane wave basis set

Let γ^a be the number of core electrons, $\zeta_j^a(\mathbf{r})$ is j^{th} core orbital, $\nu^a(\mathbf{r})$ is the core electron density, and $Z_a = Z_a \delta(\mathbf{r} - \mathbf{P}_a)$ is the nuclear charge density of the atom a . The constant term in the Hamiltonian is

$$(B.1) \quad H^{(0)} = 2 \sum_{a=1}^{N_A} \sum_{j=1}^{\gamma_c^a/2} \langle \zeta_j^a | -\frac{1}{2} \nabla^2 | \zeta_j^a \rangle + \sum_{aa'}' \frac{1}{2} (\nu^a + Z_a | \nu^{a'} + Z_{a'}) - \sum_{aa'} \sum_{jk}^{\gamma^a/2} (\zeta_k^{a'} \zeta_j^{*a} | \zeta_k^{*a'} \zeta_j^a),$$

where prime over the sum indicates that the self-interaction energy is not included, and where we introduced the notation

$$(B.2) \quad (f|g) = \iint d^3\mathbf{r} d^3\mathbf{r}' \frac{f^*(\mathbf{r}')g(\mathbf{r})}{|\mathbf{r}' - \mathbf{r}|}.$$

The one-body matrix elements consist of the valence electron kinetic and external potential contributions, the interaction of valence electrons with core electrons, and the PAW correction:

$$(B.3) \quad h_{pq} = -\frac{1}{2} \int_V d^3\mathbf{r} \tilde{\psi}_p^*(\mathbf{r}) \nabla^2 \tilde{\psi}_q(\mathbf{r}) - \sum_{a=1}^{N_A} Z_a \int_V d^3\mathbf{r} \frac{\tilde{\rho}_{pq}(\mathbf{r})}{|\mathbf{r} - \mathbf{P}_a|} + \sum_{a=1}^{N_A} \frac{\gamma^a}{\sqrt{4\pi}} (\tilde{g}_0^a | \tilde{\rho}_{pq}) + \sum_{a=1}^{N_A} \sum_{i_1 i_2}^{n_a} D_{pq, i_1 i_2}^a [H_{i_1 i_2}^a + V_{i_1 i_2}^a - X_{i_1 i_2}^a],$$

where

$$(B.4) \quad \tilde{\rho}_{pq}(\mathbf{r}) = \tilde{n}_{pq}(\mathbf{r}) + \sum_{a=1}^{N_A} \tilde{Z}_{pq}^a(\mathbf{r}), \quad \tilde{n}_{pq}(\mathbf{r}) = \tilde{\psi}_p^*(\mathbf{r}) \tilde{\psi}_q(\mathbf{r}),$$

$$(B.5) \quad \tilde{Z}_{pq}^a(\mathbf{r}) = \sum_{L=0}^{L_{\text{max}}} Q_{pq,L}^a \tilde{g}_L^a(\mathbf{r}), \quad Q_{pq,L}^b = \sum_{i_1 i_2}^{n_a} \Delta_{L i_1 i_2}^a D_{pq, i_1 i_2}^a.$$

where $D_{pq, i_1 i_2}^a$ is the atomic orbital-pair density matrix:

$$(B.6) \quad D_{pq, i_1 i_2}^a = \langle \tilde{\psi}_p | p_{i_1}^a \rangle \langle p_{i_2}^a | \tilde{\psi}_q \rangle$$

The atomic compensation charges $\sum_a Z_{pq}^a(\mathbf{r})$ are introduced to ensure that the Coulomb potential created by atomic-centered densities are zero outside the augmentation spheres, which allows for separation of the original Hamiltonian into soft and atomic parts only. The same approach will be used below for the two-body term. The atomic constants

due to the kinetic energy and external potential contribution, $H_{i_1 i_2}^a$, the Hartree energy of valence and core electrons, $V_{i_1 i_2}^a$, and the exchange energy between valence and core electrons, $X_{i_1 i_2}^a$, are

$$(B.7) \quad H_{i_1 i_2}^a = \langle \phi_{i_1}^a | -\frac{1}{2}\nabla^2 - \frac{Z_a}{|\mathbf{r} - \mathbf{P}_a|} | \phi_{i_2}^a \rangle - \langle \tilde{\phi}_{i_1}^a | -\frac{1}{2}\nabla^2 - \frac{Z_a}{|\mathbf{r} - \mathbf{P}_a|} | \tilde{\phi}_{i_2}^a \rangle.$$

$$(B.8) \quad V_{i_1 i_2}^a = (\phi_{i_1}^a \phi_{i_2}^a | n^{a,\text{core}}) - \frac{\gamma^a}{\sqrt{4\pi}} (\tilde{\phi}_{i_1}^a \tilde{\phi}_{i_2}^a | \tilde{g}_0^a) - \frac{\gamma^a}{\sqrt{4\pi}} (\tilde{g}_0^a | \tilde{g}_0^a) \Delta_{0, i_1 i_2}^a,$$

$$(B.9) \quad X_{i_1 i_2}^a = \sum_{j=1}^{\gamma^a/2} (\phi_{i_1}^a \zeta_j^a | \phi_{i_2}^a \zeta_j^a),$$

and $\tilde{g}_L^a(\mathbf{r})$ is a Gaussian function localized on atom a , with angular and magnetic numbers $L = (l, m)$. We note that there are approaches which parameterize the all-electron one-body term [86] in different way using Fock matrix, but the approach of Ref. [86] requires implementation of the additional term that accounts for double-counting. The two-body term is

$$(B.10) \quad \kappa_{pqrs} = (\tilde{\rho}_{pq} | \tilde{\rho}_{rs}) + \sum_a^{N_A} \sum_{i_1 i_2 i_3 i_4}^{n_a} C_{i_1 i_2 i_3 i_4}^a D_{pq, i_1 i_2}^{a*} D_{rs, i_3 i_4}^a.$$

The matrix element is expanded into a sum of the soft contribution and atomic PAW correction. The definition of the coefficient $C_{i_1 i_2 i_3 i_4}^a$ is given in Ref. [39]. The most computationally intensive part for calculating matrix elements for such a Hamiltonian is the soft two-body contribution since it is a 4-rank tensor. We will use a plane-wave basis set in order to derive an LCU decomposition of the two-body term.

1. Factorization of soft two-body term using plane waves

The soft part of the two-body term can be expanded as:

$$(B.11) \quad \tilde{\kappa}_{pqrs} = (\tilde{\rho}_{pq} | \tilde{\rho}_{rs}) = \sum_j (\eta_{pq,j} | \eta_{rs,j})$$

where

$$(B.12) \quad \eta_{pq,0}(\mathbf{r}) = \frac{\tilde{\rho}_{pq}(\mathbf{r}) + \tilde{\rho}_{pq}(-\mathbf{r})}{2}, \quad \eta_{pq,0}(\mathbf{r}) = \eta_{pq,0}(-\mathbf{r}) = \eta_{qp,0}^*(\mathbf{r})$$

and

$$(B.13) \quad \eta_{pq,1}(\mathbf{r}) = \frac{\tilde{\rho}_{pq}(\mathbf{r}) - \tilde{\rho}_{pq}(-\mathbf{r})}{2i}, \quad \eta_{pq,1}(\mathbf{r}) = -\eta_{pq,1}(-\mathbf{r}) = \eta_{qp,1}^*(\mathbf{r}).$$

It is convenient to introduce the orbital-pair densities, $\eta_{pq,j}$, because their plane wave coefficients (defined in Appendix D) are Hermitian matrices with reflection and anti-reflection symmetry, respectively:

$$(B.14) \quad C_{pq,j}^*(\mathbf{G}) = C_{qp,j}(\mathbf{G}), \quad C_{pq,j}(-\mathbf{G}) = (-1)^j C_{pq,j}(\mathbf{G}),$$

unlike the plane-wave coefficients of the pair-density matrix, $\rho_{pq}(\mathbf{r})$, which satisfy the following:

$$(B.15) \quad C_{pq}^*(\mathbf{G}) = C_{qp}(-\mathbf{G}).$$

Then, we use the plane-wave expansion of the Coulomb potential

$$(B.16) \quad \frac{1}{|\mathbf{r}|} = \sum_{\mathbf{G}} e^{i\mathbf{G}\mathbf{r}} v(\mathbf{G})$$

to derive

$$(B.17) \quad \tilde{\kappa}_{pqrs} = 2 \sum_{j=1,2} \sum_{\mathbf{G} \geq 0} v'(\mathbf{G}) C_{pq,j}^*(\mathbf{G}) C_{rs,j}(\mathbf{G}),$$

with $v'(0) = v(0)/2$, and $v'(\mathbf{G}) = v(\mathbf{G})$ otherwise. As one can see, we do not omit the zero \mathbf{G} component and instead will use Wigner-Seitz regularization [45].

The soft two-body term can then be rewritten as follows:

$$(B.18) \quad \hat{H}^{(2)} = \sum_j \sum_{\mathbf{G} \geq 0} v'(\mathbf{G}) \left(\sum_{pq} C_{pq,j}(\mathbf{G}) \hat{E}_{pq} \right)^2$$

We can further diagonalize $C_{pq,j}(\mathbf{G})$ using the fact that for a given \mathbf{G} it is a Hermitian matrix:

$$(B.19) \quad C_{pq,j}(\mathbf{G}) = \sum_r U_{pr,j}(\mathbf{G}) f_{r,j}(\mathbf{G}) U_{qr,j}^*(\mathbf{G}),$$

then the soft two-body term can be rewritten using free-fermionic unitaries, $\hat{U}_j(\mathbf{G})$ as follows [33]:

$$(B.20) \quad \hat{H}^{(2)} = \sum_{\mathbf{G} \geq 0} \sum_{j=1,2}^{N_{pw}/2} v'(\mathbf{G}^2) \hat{U}_j(\mathbf{G}) \left(\sum_p^{N_b} f_{p,j}(\mathbf{G}) \hat{E}_{pp} \right)^2 \hat{U}_j^\dagger(\mathbf{G})$$

2. Factorization of PAW two-body part

In order to factorize the PAW two-body term, we use the fact that the atomic Coulomb coefficients $C_{i_1 i_2 i_3 i_4}^a$ are symmetric with respect to swapping of a pair of indices (i_1, i_2) and (i_3, i_4) . Unlike the electron repulsion integrals, $C_{i_1 i_2 i_3 i_4}^a$ are not positive definite and one cannot use Cholesky decomposition which is usually used in the single- and double-factorization methods. Instead one could use a singular-value decomposition but in order to reduce the number of angles that need to be loaded from QROAM, we use regular eigendecomposition and later will simply load the sign of each term in the LCU.

By introducing the eigendecomposition

$$(B.21) \quad \left(\frac{1}{2}\right)^{\delta_{i_1 i_2} + \delta_{i_3 i_4}} C_{i_1 i_2 i_3 i_4}^a = \sum_{k \leq l} O_{i_1 i_2 k l} \epsilon_{kl} O_{i_3 i_4 k l}, \quad \text{for } i_1 \leq i_2; i_3 \leq i_4,$$

we can rewrite the PAW two-body term as follows:

$$(B.22) \quad \hat{H}^{(2),\text{PAW}} = \sum_a^{N_A} \sum_{pqrs}^{N_b} \sum_{i_1 i_2 i_3 i_4}^{n_p^a} C_{i_1 i_2 i_3 i_4}^a D_{pq,i_1 i_2}^{a*} D_{rs,i_3 i_4}^a \hat{E}_{pq}^\dagger \hat{E}_{rs} = \sum_a^{N_A} \sum_{i_1 \leq i_2} \epsilon_{i_1 i_2}^a \left(\sum_{rs} \sum_{i_3 \leq i_4} O_{i_3 i_4 i_1 i_2}^a (D_{rs,i_3 i_4}^a + D_{sr,i_3 i_4}^{a*}) \hat{E}_{rs} \right)^2.$$

Since the matrix

$$(B.23) \quad L_{pq,i_1 i_2}^a = \sum_{i_3 \leq i_4} O_{i_3 i_4 i_1 i_2}^a (D_{pq,i_3 i_4}^a + D_{qp,i_3 i_4}^{a*}),$$

is Hermitian with respect to p, q , we can make use of the additional eigendecomposition

$$(B.24) \quad L_{pq,i_1 i_2}^a = \sum_r U_{pr,i_1 i_2}^a f_{r,i_1 i_2}^a U_{qr,i_1 i_2}^a$$

and introducing the free fermionic unitaries, $\hat{U}_{i_1 i_2}^a$, we arrive at

$$(B.25) \quad \hat{H}^{(2),\text{PAW}} = \sum_a \sum_{i_1 \leq i_2} \text{sign}(\epsilon_{i_1 i_2}^a) \hat{U}_{i_1 i_2}^a \left(\sqrt{|\epsilon_{i_1 i_2}^a|} \sum_{r,\sigma} f_{r,i_1 i_2}^a \hat{n}_{r\sigma} \right)^2 \hat{U}_{i_1 i_2}^{a\dagger}$$

Appendix C: Quantum Error Correction

The algorithms presented here require coherence times and noise levels that are beyond the reach of any qubit technology, and require fully fault-tolerant quantum computation. To achieve this we use Quantum Error Correction (QEC), where many physical qubits are used to encode a single logical qubit. In [87, Section 4] we detail the error correction scheme we use, which is based on the surface code on a 2D grid, following the scheme given in “A Game of Surface Codes” [88].

We choose a target failure probability of $p_{\text{fail}} = 1\%$ for a full execution of the quantum algorithm, which we divide into error budgets $p_{\text{fail}}^{\text{log}} = 0.9\%$ for logical errors, and $p_{\text{fail}}^{\text{MSD}} = 0.1\%$ for undetected errors in magic state distillation.

Due to the large number of Toffoli gates required for this algorithm, we utilise gate synthillation in magic state factories that produce CCZ states [89–93] instead of T factories. Gate synthillation allows us to produce $|\text{CCZ}\rangle$ states with a lower overhead than producing four T states to implement a Toffoli gate. For the largest systems considered here, we use the $(15\text{-to-}1)_{9,3,3}^4 \times (8\text{-to-CZZ})_{25,9,9}$ factory from [93]. It has a sufficiently low failure probability, below the target error $p_{\text{fail}}^{\text{MSD}}/N_{\text{Toff}}$ for the largest system; we can use smaller factories for smaller instances. A smaller code distance than d in the logical computation can be used for the magic state factory to reduce its footprint and runtime. In fact, rectangular code patches with distinct distances for X, Z, and time (as indicated by the subscripts) can be used as the factory is more prone to some types of error than others.

Like in [87] we assume the computation proceeds as fast as consuming one magic state qubit per logical clock cycle, where a logical clock cycle is equivalent to d code cycles, and d is the code distance. Consequently, we ensure that the number of magic state factories available is high enough that a single magic state is available every three logical cycles, which typically requires multiple magic state factories. The length of the computation is $3N_{\text{Toff}}$ logical cycles.

The logical error budget bounds the allowed logical failure probability per logical cycle, which is given by the Fowler-Devitt-Jones formula [94]. Hence the computational code distance d must be chosen such that

$$(C.1) \quad A \left(\frac{p}{p_{\text{thr}}} \right)^{\frac{d+1}{2}} \leq \frac{p_{\text{fail}}^{\text{log}}}{3N_{\text{Toff}}N_{\text{qubits}}},$$

where p is the probability of a physical error, $p_{\text{thr}} \approx 0.01$ is the threshold of the surface code, and $A = 0.1$ is a numerically determined constant.

In order to estimate the physical resources, we model a 2D superconducting device as in [87], with an error rate one order of magnitude better than current superconducting devices [95, 96], i.e. $p = 0.01\%$. This allows us to solve Equation C.1 for d . The total number of logical qubits n_L is given by the number of qubits required by the algorithm and the routing required by the *fast-block* layout [88, Figure 13]. The total number of physical qubits is then $(2d^2 - 1)n_L$ for algorithm and routing in the rotated surface code, together with those required by the magic state factories.

Appendix D: Properties of reciprocal pair densities

We define the plane wave expansion for a periodic function as

$$(D.1) \quad f(\mathbf{r}) = \sum_{\mathbf{G}} e^{i\mathbf{G}\mathbf{r}} C(\mathbf{G}),$$

where

$$(D.2) \quad C(\mathbf{G}) = \frac{1}{V} \int_V d^3\mathbf{r} e^{-i\mathbf{G}\mathbf{r}} f(\mathbf{r}).$$

1. Complex orbital-pair densities

For complex-valued orbitals (as well as real), we have the following properties for pair-densities:

$$(D.3) \quad C_{pq}^*(\mathbf{G}) = C_{qp}(-\mathbf{G}).$$

2. Real orbital-pair densities

Additionally, real orbitals satisfy

$$(D.4) \quad C_{pq}(\mathbf{G}) = C_{qp}(\mathbf{G}),$$

which leads to

$$(D.5) \quad C_{pq}(-\mathbf{G}) = C_{qp}^*(\mathbf{G}) = C_{pq}^*(\mathbf{G}).$$

Thus, we don't need to store the $-G$ component, since the coefficients can be restored by conjugation. Also, for real orbitals,

$$(D.6) \quad \eta_{pq,0} = \frac{C_{pq}(\mathbf{G}) + C_{qp}^*(\mathbf{G})}{2} = \frac{C_{pq}(\mathbf{G}) + C_{pq}^*(\mathbf{G})}{2} = \text{Re}(C_{pq}(\mathbf{G})),$$

and

$$(D.7) \quad \eta_{pq,1} = \frac{(C_{pq}(\mathbf{G}) - C_{qp}^*(\mathbf{G}))}{2i} = \frac{(C_{pq}(\mathbf{G}) - C_{pq}^*(\mathbf{G}))}{2i} = \text{Im}(C_{pq}(\mathbf{G})).$$

Appendix E: Block encoding of a squared matrix

A main feature of the double factorised Hamiltonian is that it contains terms that are a square A^2 of another expression, see (III.8). Starting from a block encoding of A/α (with subnormalisation α), in principle the square can be implemented by multiplying block-encoded matrices [32, 97, 98], yielding a block encoding $\frac{1}{\alpha^2}A^2$. Instead, when the double factorisation algorithm was conceived in [32], the square was implemented by applying the second Chebyshev polynomial

$$(E.1) \quad T_2(x) = 2x^2 - 1$$

to A/α . This results in a block encoding of $\frac{2}{\alpha^2}A^2 - 1$, whose constant shift can be computed classically. Compared to multiplication, the subnormalisation of the Chebyshev polynomial is better by a factor of 2, at the same query complexity. This factor of two has been taken into account when computing the subnormalisation (III.10).

Chebyshev polynomials can be implemented via qubitisation [25]. Here we explicitly demonstrate $T_2(x)$. Let

$$(E.2) \quad U = \begin{pmatrix} A/\alpha & B \\ B^\dagger & C \end{pmatrix}, \quad \mathcal{R} = \begin{pmatrix} \mathbb{1} & \\ & -\mathbb{1} \end{pmatrix}$$

be a Hermitian block encoding of the Hermitian A/α , and the reflection around the coding subspace. Due to unitarity we have $(A/\alpha)^2 + BB^\dagger = \mathbb{1}$, such that

$$(E.3) \quad URU = \begin{pmatrix} A/\alpha & B \\ B^\dagger & C \end{pmatrix} \begin{pmatrix} A/\alpha & B \\ -B^\dagger & -C \end{pmatrix} = \begin{pmatrix} (A/\alpha)^2 - BB^\dagger & \cdot \\ \cdot & \cdot \end{pmatrix} = \begin{pmatrix} (A/\alpha)^2 + (A/\alpha)^2 - \mathbb{1} & \cdot \\ \cdot & \cdot \end{pmatrix} = \begin{pmatrix} 2(A/\alpha)^2 - \mathbb{1} & \cdot \\ \cdot & \cdot \end{pmatrix},$$

where we have omitted calculation of the junk blocks of the final block encoding. The reflection \mathcal{R} must implement a -1 phase outside of the coding subspace, otherwise $-T_2(x)$ is implemented. To this end, we have added a CZ to the implementation of the reflection in Fig. 2.

-
- [1] R. Izsák, A. V. Ivanov, N. S. Blunt, N. Holzmann and F. Neese, *Measuring electron correlation: The impact of symmetry and orbital transformations*, Journal of Chemical Theory and Computation **19**(10), 2703 (2023), doi:10.1021/acs.jctc.3c00122.
 - [2] S. Lee, J. Lee, H. Zhai, Y. Tong, A. M. Dalzell, A. Kumar, P. Helms, J. Gray, Z.-H. Cui, W. Liu *et al.*, *Evaluating the evidence for exponential quantum advantage in ground-state quantum chemistry*, Nature communications **14**(1), 1952 (2023), doi:10.1038/s41467-023-37587-6.
 - [3] W. Kohn and L. J. Sham, *Self-Consistent Equations Including Exchange and Correlation Effects*, Physical Review **140**(4A), A1133 (1965), doi:10.1103/PhysRev.140.A1133.
 - [4] C. C. J. Roothaan, *New developments in molecular orbital theory*, Rev. Mod. Phys. **23**, 69 (1951), doi:10.1103/RevModPhys.23.69.

- [5] S. F. Boys and A. C. Egerton, *Electronic wave functions - i. a general method of calculation for the stationary states of any molecular system*, Proceedings of the Royal Society of London. Series A. Mathematical and Physical Sciences **200**(1063), 542 (1950), doi:10.1098/rspa.1950.0036.
- [6] S. Raimes, *The wave mechanics of electrons in metals*, North-Holland Publishing Company, Amsterdam (1961).
- [7] L. Talirz, L. M. Ghiringhelli and B. Smit, *Trends in atomistic simulation software usage*, Living Journal of Computational Molecular Science **3**(1) (2021), doi:10.33011/livecoms.3.1.1483, ArXiv:2108.12350 [cond-mat, physics:physics].
- [8] I. D. Kivlichan, C. Gidney, D. W. Berry, N. Wiebe, J. McClean, W. Sun, Z. Jiang, N. Rubin, A. Fowler, A. Aspuru-Guzik, H. Neven and R. Babbush, *Improved Fault-Tolerant Quantum Simulation of Condensed-Phase Correlated Electrons via Trotterization*, Quantum **4**, 296 (2020), doi:10.22331/q-2020-07-16-296.
- [9] R. Babbush, C. Gidney, D. W. Berry, N. Wiebe, J. McClean, A. Paler, A. Fowler and H. Neven, *Encoding Electronic Spectra in Quantum Circuits with Linear T Complexity*, Physical Review X **8**(4), 041015 (2018), doi:10.1103/PhysRevX.8.041015, Publisher: American Physical Society.
- [10] R. Babbush, N. Wiebe, J. McClean, J. McClain, H. Neven and G. K.-L. Chan, *Low-Depth Quantum Simulation of Materials*, Physical Review X **8**(1), 011044 (2018), doi:10.1103/PhysRevX.8.011044.
- [11] F. Gygi, *All-Electron Plane-Wave Electronic Structure Calculations*, Journal of Chemical Theory and Computation **19**(4), 1300 (2023), doi:10.1021/acs.jctc.2c01191.
- [12] D. R. Hamann, M. Schlüter and C. Chiang, *Norm-conserving pseudopotentials*, Phys. Rev. Lett. **43**, 1494 (1979), doi:10.1103/PhysRevLett.43.1494.
- [13] D. Vanderbilt, *Soft self-consistent pseudopotentials in a generalized eigenvalue formalism*, Phys. Rev. B **41**, 7892 (1990), doi:10.1103/PhysRevB.41.7892.
- [14] P. E. Blöchl, *Projector augmented-wave method*, Phys. Rev. B **50**, 17953 (1994), doi:10.1103/PhysRevB.50.17953.
- [15] G. Prandini, A. Marrazzo, I. E. Castelli, N. Mounet and N. Marzari, *Precision and efficiency in solid-state pseudopotential calculations*, npj Computational Materials **4**(1), 72 (2018), doi:10.1038/s41524-018-0127-2, <http://materialscloud.org/sssip>.
- [16] J. Paier, R. Hirschl, M. Marsman and G. Kresse, *The Perdew–Burke–Ernzerhof exchange-correlation functional applied to the G2-1 test set using a plane-wave basis set*, The Journal of Chemical Physics **122**(23), 234102 (2005), doi:10.1063/1.1926272.
- [17] M. Humer, M. E. Harding, M. Schlipf, A. Taheridehkordi, Z. Sukurma, W. Klopper and G. Kresse, *Approaching the basis-set limit of the dRPA correlation energy with explicitly correlated and projector augmented-wave methods*, The Journal of Chemical Physics **157**(19), 194113 (2022), doi:10.1063/5.0124019.
- [18] K. Lejaeghere, G. Bihlmayer, T. Björkman, P. Blaha, S. Blügel, V. Blum, D. Caliste, I. E. Castelli, S. J. Clark, A. Dal Corso, S. de Gironcoli, T. Deutsch *et al.*, *Reproducibility in density functional theory calculations of solids*, Science **351**(6280), aad3000 (2016), doi:10.1126/science.aad3000.
- [19] E. Bosoni, L. Beal, M. Bercx, P. Blaha, S. Blügel, J. Bröder, M. Callsen, S. Cottenier, A. Degomme, V. Dikan, K. Eimre, E. Flage-Larsen *et al.*, *How to verify the precision of density-functional-theory implementations via reproducible and universal workflows*, Nature Reviews Physics **6**(1), 45 (2023), doi:10.1038/s42254-023-00655-3.
- [20] S. Goedecker, M. Teter and J. Hutter, *Separable dual-space Gaussian pseudopotentials*, Physical Review B **54**(3), 1703 (1996), doi:10.1103/PhysRevB.54.1703.
- [21] C. Hartwigsen, S. Goedecker and J. Hutter, *Relativistic separable dual-space Gaussian Pseudopotentials from H to Rn* , Physical Review B **58**(7), 3641 (1998), doi:10.1103/PhysRevB.58.3641, ArXiv:cond-mat/9803286.
- [22] Y. Su, D. W. Berry, N. Wiebe, N. Rubin and R. Babbush, *Fault-Tolerant Quantum Simulations of Chemistry in First Quantization*, Physical Review X Quantum **2**(4), 040332 (2021), doi:10.1103/PRXQuantum.2.040332.
- [23] M. S. Zini, A. Delgado, R. d. Reis, P. A. M. Casares, J. E. Mueller, A.-C. Voigt and J. M. Arrazola, *Quantum simulation of battery materials using ionic pseudopotentials*, Quantum **7**, 1049 (2023), doi:10.22331/q-2023-07-10-1049, ArXiv:2302.07981 [cond-mat, physics:quant-ph].
- [24] D. W. Berry, N. C. Rubin, A. O. Elnabawy, G. Ahlers, A. E. DePrince III, J. Lee, C. Gogolin and R. Babbush, *Quantum Simulation of Realistic Materials in First Quantization Using Non-local Pseudopotentials*, ArXiv:2312.07654 [quant-ph] (2023).
- [25] G. H. Low and I. L. Chuang, *Hamiltonian Simulation by Qubitization*, Quantum **3**, 163 (2019), doi:10.22331/q-2019-07-12-163, ArXiv:1610.06546 [quant-ph].
- [26] D. Poulin, A. Kitaev, D. S. Steiger, M. B. Hastings and M. Troyer, *Quantum Algorithm for Spectral Measurement with Lower Gate Count*, Physical Review Letters **121**(1), 010501 (2018), doi:10.1103/PhysRevLett.121.010501, ArXiv:1711.11025.
- [27] D. W. Berry, M. Kieferová, A. Scherer, Y. R. Sanders, G. H. Low, N. Wiebe, C. Gidney and R. Babbush, *Improved techniques for preparing eigenstates of fermionic Hamiltonians*, npj Quantum Information **4**(1), 22 (2018), doi:10.1038/s41534-018-0071-5.
- [28] A. Y. Kitaev, *Quantum measurements and the abelian stabilizer problem*, arXiv:quant-ph/9511026 (1995), doi:10.48550/arxiv.quant-ph/9511026.
- [29] M. A. Nielsen and I. L. Chuang, *Quantum computation and quantum information*, Cambridge University Press, Cambridge ; New York, 10th edn., ISBN 978-1-107-00217-3 (2010).
- [30] G. H. Low, V. Kliuchnikov and L. Schaeffer, *Trading t -gates for dirty qubits in state preparation and unitary synthesis* (2018), 1812.00954.
- [31] D. W. Berry, C. Gidney, M. Motta, J. R. McClean and R. Babbush, *Qubitization of Arbitrary Basis Quantum Chemistry Leveraging Sparsity and Low Rank Factorization*, Quantum **3**, 208 (2019), doi:10.22331/q-2019-12-02-208.
- [32] V. von Burg, G. H. Low, T. Häner, D. S. Steiger, M. Reiher, M. Roetteler and M. Troyer, *Quantum computing en-*

- hanced computational catalysis*, Physical Review Research **3**(3), 033055 (2021), doi:10.1103/PhysRevResearch.3.033055, ArXiv:2007.14460 [physics, physics:quant-ph].
- [33] J. Lee, D. W. Berry, C. Gidney, W. J. Huggins, J. R. McClean, N. Wiebe and R. Babbush, *Even More Efficient Quantum Computations of Chemistry Through Tensor Hypercontraction*, PRX Quantum **2**(3), 030305 (2021), doi:10.1103/PRXQuantum.2.030305.
- [34] A. V. Ivanov, C. Sünderhauf, N. Holzmann, T. Ellaby, R. N. Kerber, G. Jones and J. Camps, *Quantum computation for periodic solids in second quantization*, Physical Review Research **5**(1), 013200 (2023), doi:10.1103/PhysRevResearch.5.013200.
- [35] N. C. Rubin, D. W. Berry, F. D. Malone, A. F. White, T. Khattar, A. E. DePrince, S. Siculo, M. Kühn, M. Kaicher, J. Lee and R. Babbush, *Fault-Tolerant Quantum Simulation of Materials Using Bloch Orbitals*, PRX Quantum **4**(4), 040303 (2023), doi:10.1103/PRXQuantum.4.040303.
- [36] J. J. Mortensen, A. H. Larsen, M. Kuisma, A. V. Ivanov, A. Taghizadeh, A. Peterson, A. Haldar, A. O. Dohn, C. Schäfer, E. O. Jónsson, E. D. Hermes, F. A. Nilsson *et al.*, *GPAW: open Python package for electronic-structure calculations*, ArXiv:2310.14776 [cond-mat, physics:physics] (2023).
- [37] Y.-y. Ohnishi and S. Hirata, *Logarithm second-order many-body perturbation method for extended systems*, The Journal of Chemical Physics **133**(3), 034106 (2010), doi:10.1063/1.3455717.
- [38] A. Grüneis, G. H. Booth, M. Marsman, J. Spencer, A. Alavi and G. Kresse, *Natural Orbitals for Wave Function Based Correlated Calculations Using a Plane Wave Basis Set*, Journal of Chemical Theory and Computation **7**(9), 2780 (2011), doi:10.1021/ct200263g.
- [39] C. Rostgaard, *The projector augmented-wave method*, doi:10.48550/arxiv.0910.1921 (2009).
- [40] D. R. Hamann, *Optimized norm-conserving Vanderbilt pseudopotentials*, Physical Review B **88**(8), 085117 (2013), doi:10.1103/PhysRevB.88.085117.
- [41] I. Mayer, *Simple theorems, proofs, and derivations in quantum chemistry*, Springer Science & Business Media (2003).
- [42] S. Huzinaga and A. A. Cantu, *Theory of Separability of Many-Electron Systems*, The Journal of Chemical Physics **55**(12), 5543 (1971), doi:10.1063/1.1675720.
- [43] J. Paldus, *The unitary group for the evaluation of electronic energy matrix elements*, In *The Unitary Group for the Evaluation of Electronic Energy Matrix Elements*, pp. 1–50. Springer, Berlin (1981).
- [44] F. Aquilante, T. K. Todorova, L. Gagliardi, T. B. Pedersen and B. O. Roos, *Systematic truncation of the virtual space in multiconfigurational perturbation theory*, The Journal of Chemical Physics **131**(3), 034113 (2009), doi:10.1063/1.3157463.
- [45] R. Sundararaman and T. A. Arias, *Regularization of the coulomb singularity in exact exchange by wigner-seitz truncated interactions: Towards chemical accuracy in nontrivial systems*, Phys. Rev. B **87**, 165122 (2013), doi:10.1103/PhysRevB.87.165122.
- [46] M. Motta, E. Ye, J. R. McClean, Z. Li, A. J. Minnich, R. Babbush and G. K.-L. Chan, *Low rank representations for quantum simulation of electronic structure*, npj Quantum Information **7**(1), 83 (2021), doi:10.1038/s41534-021-00416-z.
- [47] J. R. McClean, N. C. Rubin, K. J. Sung, I. D. Kivlichan, X. Bonnet-Monroig, Y. Cao, C. Dai, E. S. Fried, C. Gidney, B. Gimby *et al.*, *Openfermion: the electronic structure package for quantum computers*, Quantum Science and Technology **5**(3), 034014 (2020).
- [48] <https://molmod.ugent.be/deltacodesdft>.
- [49] K. Lejaeghere, V. Van Speybroeck, G. Van Oost and S. Cottenier, *Error Estimates for Solid-State Density-Functional Theory Predictions: An Overview by Means of the Ground-State Elemental Crystals*, Critical Reviews in Solid State and Materials Sciences **39**(1), 1 (2014), doi:10.1080/10408436.2013.772503.
- [50] B. O. Roos, R. Lindh, P.-A. Malmqvist, V. Veryazov and P.-O. Widmark, *Main Group Atoms and Dimers Studied with a New Relativistic ANO Basis Set*, The Journal of Physical Chemistry A **108**(15), 2851 (2004), doi:10.1021/jp031064+.
- [51] B. P. Pritchard, D. Altarawy, B. Didier, T. D. Gibson and T. L. Windus, *New Basis Set Exchange: An Open, Up-to-Date Resource for the Molecular Sciences Community*, Journal of Chemical Information and Modeling **59**(11), 4814 (2019), doi:10.1021/acs.jcim.9b00725.
- [52] K. L. Schuchardt, B. T. Didier, T. Elsethagen, L. Sun, V. Gurumoorthi, J. Chase, J. Li and T. L. Windus, *Basis Set Exchange: A Community Database for Computational Sciences*, Journal of Chemical Information and Modeling **47**(3), 1045 (2007), doi:10.1021/ci600510j.
- [53] D. Feller, *The role of databases in support of computational chemistry calculations*, Journal of Computational Chemistry **17**(13), 1571 (1996), doi:10.1002/(SICI)1096-987X(199610)17:13<1571::AID-JCC9>3.0.CO;2-P.
- [54] Q. Sun, X. Zhang, S. Banerjee, P. Bao, M. Barbry, N. S. Blunt, N. A. Bogdanov, G. H. Booth, J. Chen, Z.-H. Cui, J. J. Eriksen, Y. Gao *et al.*, *Recent developments in the PySCF program package*, The Journal of Chemical Physics **153**(2), 024109 (2020), doi:10.1063/5.0006074.
- [55] Q. Sun, T. C. Berkelbach, N. S. Blunt, G. H. Booth, S. Guo, Z. Li, J. Liu, J. D. McClain, E. R. Sayfutyarova, S. Sharma, S. Wouters and G. K. Chan, *PySCF: the Python-based simulations of chemistry framework*, WIREs Computational Molecular Science **8**(1), e1340 (2018), doi:10.1002/wcms.1340.
- [56] Q. Sun, *Libcint: An efficient general integral library for Gaussian basis functions*, Journal of Computational Chemistry **36**(22), 1664 (2015), doi:10.1002/jcc.23981.
- [57] J. Enkovaara, C. Rostgaard, J. J. Mortensen, J. Chen, M. Dulák, L. Ferrighi, J. Gavnholt, C. Glinsvad, V. Haikola, H. A. Hansen, H. H. Kristoffersen, M. Kuisma *et al.*, *Electronic structure calculations with GPAW: a real-space implementation of the projector augmented-wave method*, Journal of Physics: Condensed Matter **22**(25), 253202 (2010), doi:10.1088/0953-8984/22/25/253202.
- [58] J. J. Mortensen, L. B. Hansen and K. W. Jacobsen, *Real-space grid implementation of the projector augmented wave method*, Physical Review B **71**(3), 035109 (2005), doi:10.1103/PhysRevB.71.035109.

- [59] http://www.quantum-simulation.org/potentials/sg15_oncvc/.
- [60] M. Krack, *Pseudopotentials for H to Kr optimized for gradient-corrected exchange-correlation functionals*, Theoretical Chemistry Accounts **114**(1-3), 145 (2005), doi:10.1007/s00214-005-0655-y.
- [61] <http://materialscloud.org/sssp>.
- [62] H. J. Monkhorst and J. D. Pack, *Special points for Brillouin-zone integrations*, Physical Review B **13**(12), 5188 (1976), doi:10.1103/PhysRevB.13.5188.
- [63] R. Schirhagl, K. Chang, M. Loretz and C. L. Degen, *Nitrogen-Vacancy Centers in Diamond: Nanoscale Sensors for Physics and Biology*, Annual Review of Physical Chemistry **65**(1), 83 (2014), doi:10.1146/annurev-physchem-040513-103659.
- [64] J. R. Maze, P. L. Stanwix, J. S. Hodges, S. Hong, J. M. Taylor, P. Cappellaro, L. Jiang, M. V. G. Dutt, E. Togan, A. S. Zibrov, A. Yacoby, R. L. Walsworth *et al.*, *Nanoscale magnetic sensing with an individual electronic spin in diamond*, Nature **455**(7213), 644 (2008), doi:10.1038/nature07279.
- [65] G. Balasubramanian, I. Y. Chan, R. Kolesov, M. Al-Hmoud, J. Tisler, C. Shin, C. Kim, A. Wojcik, P. R. Hemmer, A. Krueger, T. Hanke, A. Leitenstorfer *et al.*, *Nanoscale imaging magnetometry with diamond spins under ambient conditions*, Nature **455**(7213), 648 (2008), doi:10.1038/nature07278.
- [66] J. M. Taylor, P. Cappellaro, L. Childress, L. Jiang, D. Budker, P. R. Hemmer, A. Yacoby, R. Walsworth and M. D. Lukin, *High-sensitivity diamond magnetometer with nanoscale resolution*, Nature Physics **4**(10), 810 (2008), doi:10.1038/nphys1075.
- [67] B. Hensen, H. Bernien, A. E. Dréau, A. Reiserer, N. Kalb, M. S. Blok, J. Ruitenbergh, R. F. L. Vermeulen, R. N. Schouten, C. Abellán, W. Amaya, V. Pruneri *et al.*, *Loophole-free Bell inequality violation using electron spins separated by 1.3 kilometres*, Nature **526**(7575), 682 (2015), doi:10.1038/nature15759.
- [68] I. Aharonovich, S. Castelletto, D. A. Simpson, C.-H. Su, A. D. Greentree and S. Prawer, *Diamond-based single-photon emitters*, Reports on Progress in Physics **74**(7), 076501 (2011), doi:10.1088/0034-4885/74/7/076501.
- [69] A. Beveratos, R. Brouri, T. Gacoin, A. Villing, J.-P. Poizat and P. Grangier, *Single Photon Quantum Cryptography*, Physical Review Letters **89**(18), 187901 (2002), doi:10.1103/PhysRevLett.89.187901.
- [70] G. Waldherr, Y. Wang, S. Zaiser, M. Jamali, T. Schulte-Herbrüggen, H. Abe, T. Ohshima, J. Isoya, J. F. Du, P. Neumann and J. Wrachtrup, *Quantum error correction in a solid-state hybrid spin register*, Nature **506**(7487), 204 (2014), doi:10.1038/nature12919.
- [71] T. H. Taminiau, J. Cramer, T. van der Sar, V. V. Dobrovitski and R. Hanson, *Universal control and error correction in multi-qubit spin registers in diamond*, Nature Nanotechnology **9**(3), 171 (2014), doi:10.1038/nnano.2014.2.
- [72] M. W. Doherty, N. B. Manson, P. Delaney, F. Jelezko, J. Wrachtrup and L. C. Hollenberg, *The nitrogen-vacancy colour centre in diamond*, Physics Reports **528**(1), 1 (2013), doi:10.1016/j.physrep.2013.02.001.
- [73] J. R. Weber, W. F. Koehl, J. B. Varley, A. Janotti, B. B. Buckley, C. G. Van de Walle and D. D. Awschalom, *Quantum computing with defects*, Proceedings of the National Academy of Sciences **107**(19), 8513 (2010), doi:10.1073/pnas.1003052107.
- [74] P. Neumann, N. Mizuochi, F. Rempp, P. Hemmer, H. Watanabe, S. Yamasaki, V. Jacques, T. Gaebel, F. Jelezko and J. Wrachtrup, *Multipartite Entanglement Among Single Spins in Diamond*, Science **320**(5881), 1326 (2008), doi:10.1126/science.1157233.
- [75] A. V. Ivanov, Y. L. A. Schmerwitz, G. Levi and H. Jónsson, *Electronic excitations of the charged nitrogen-vacancy center in diamond obtained using time-independent variational density functional calculations*, SciPost Physics **15**(1), 009 (2023), doi:10.21468/SciPostPhys.15.1.009.
- [76] Y. Jin, M. Govoni and G. Galli, *Vibrationally resolved optical excitations of the nitrogen-vacancy center in diamond*, npj Computational Materials **8**(1), 1 (2022), doi:10.1038/s41524-022-00928-y.
- [77] H. Ma, M. Govoni and G. Galli, *Quantum simulations of materials on near-term quantum computers*, npj Computational Materials **6**(1), 85 (2020), doi:10.1038/s41524-020-00353-z.
- [78] Y. Ma, M. Rohlfing and A. Gali, *Excited states of the negatively charged nitrogen-vacancy color center in diamond*, Physical Review B **81**(4), 041204 (2010), doi:10.1103/PhysRevB.81.041204.
- [79] K. A. Simula and I. Makkonen, *Calculation of the energies of the multideterminant states of the nitrogen vacancy center in diamond with quantum monte carlo*, Phys. Rev. B **108**, 094108 (2023), doi:10.1103/PhysRevB.108.094108.
- [80] S. Haldar, A. Mitra, M. R. Hermes and L. Gagliardi, *Local Excitations of a Charged Nitrogen Vacancy in Diamond with Multireference Density Matrix Embedding Theory*, The Journal of Physical Chemistry Letters **14**(18), 4273 (2023), doi:10.1021/acs.jpcclett.3c00551.
- [81] C. Bhandari, A. L. Wysocki, S. E. Economou, P. Dev and K. Park, *Multiconfigurational study of the negatively charged nitrogen-vacancy center in diamond*, Physical Review B **103**(1), 014115 (2021), doi:10.1103/PhysRevB.103.014115.
- [82] J. S. Baker, P. A. M. Casares, M. S. Zini, J. Thik, D. Banerjee, C. Ling, A. Delgado and J. M. Arrazola, *Simulating optically-active spin defects with a quantum computer*, ArXiv:2405.13115 [cond-mat, physics:quant-ph] (2024).
- [83] L. Muechler, D. I. Badrtdinov, A. Hampel, J. Cano, M. Rösner and C. E. Dreyer, *Quantum embedding methods for correlated excited states of point defects: Case studies and challenges*, Physical Review B **105**(23), 235104 (2022), doi:10.1103/PhysRevB.105.235104.
- [84] R. Babbush, D. W. Berry, J. R. McClean and H. Neven, *Quantum simulation of chemistry with sublinear scaling in basis size*, npj Quantum Information **5**(1), 92 (2019), doi:10.1038/s41534-019-0199-y.
- [85] T. N. Georges, M. Bothe, C. Sünderhauf, B. K. Berntson, R. Izsák and A. V. Ivanov, *Quantum Simulations of Chemistry in First Quantization with any Basis Set* (2024).
- [86] Y. L. A. Schmerwitz, L. Thirion, G. Levi, E. O. Jónsson, P. Bilous, H. Jónsson and P. Hansmann, *Revisiting N₂ with Neural-Network-Supported CI*, ArXiv:2406.08154 [physics] (2024).
- [87] N. S. Blunt, J. Camps, O. Crawford, R. Izsák, S. Leontica, A. Mirani, A. E. Moylett, S. A. Scivier, C. Sünderhauf,

- P. Schopf, J. M. Taylor and N. Holzmann, *Perspective on the Current State-of-the-Art of Quantum Computing for Drug Discovery Applications*, Journal of Chemical Theory and Computation **18**(12), 7001 (2022), doi:10.1021/acs.jctc.2c00574.
- [88] D. Litinski, *A Game of Surface Codes: Large-Scale Quantum Computing with Lattice Surgery*, Quantum **3**, 128 (2019), doi:10.22331/q-2019-03-05-128.
- [89] C. Jones, *Novel constructions for the fault-tolerant Toffoli gate*, Physical Review A **87**(2), 022328 (2013), doi:10.1103/PhysRevA.87.022328, 1212.5069.
- [90] B. Eastin, *Distilling one-qubit magic states into Toffoli states*, Physical Review A **87**(3), 032321 (2013), doi:10.1103/PhysRevA.87.032321.
- [91] E. T. Campbell and M. Howard, *Unified framework for magic state distillation and multiqubit gate synthesis with reduced resource cost*, Physical Review A **95**(2), 022316 (2017), doi:10.1103/PhysRevA.95.022316.
- [92] C. Gidney and A. G. Fowler, *Efficient magic state factories with a catalyzed $|CCZ\rangle$ to $2|T\rangle$ transformation*, Quantum **3** (2019), doi:10.22331/q-2019-04-30-135.
- [93] D. Litinski, *Magic State Distillation: Not as Costly as You Think*, arXiv:1905.06903 [quant-ph] (2019), 1905.06903.
- [94] A. G. Fowler, M. Mariantoni, J. M. Martinis and A. N. Cleland, *Surface codes: Towards practical large-scale quantum computation*, Physical Review A - Atomic, Molecular, and Optical Physics **86**(3) (2012), doi:10.1103/PhysRevA.86.032324.
- [95] Google Quantum AI, R. Acharya, I. Aleiner, R. Allen, T. I. Andersen, M. Ansmann, F. Arute, K. Arya, A. Asfaw, J. Atalaya, R. Babbush, D. Bacon *et al.*, *Suppressing quantum errors by scaling a surface code logical qubit*, Nature **614**(7949), 676 (2023), doi:10.1038/s41586-022-05434-1.
- [96] S. Krinner, N. Lacroix, A. Remm, A. Di Paolo, E. Genois, C. Leroux, C. Hellings, S. Lazar, F. Swiadek, J. Herrmann, G. J. Norris, C. K. Andersen *et al.*, *Realizing repeated quantum error correction in a distance-three surface code*, Nature **605**(7911), 669 (2022), doi:10.1038/s41586-022-04566-8.
- [97] A. Gilyén, Y. Su, G. H. Low and N. Wiebe, *Quantum singular value transformation and beyond: exponential improvements for quantum matrix arithmetics*, In *Proceedings of the 51st Annual ACM SIGACT Symposium on Theory of Computing*, pp. 193–204 (2019).
- [98] C. Sünderhauf, *Generalized quantum singular value transformation* (2023), 2312.00723.